THESIS APPROVAL

GRADUATE SCHOOL, KASETSART UNIVERSITY

Master of Science (Chemistry)

DEGREE

Chemistry	Chemistry
FIELD	**DEPARTMENT**

TITLE: Synthesis and Characterization of 1-D Nanostructured TiO_2 on FTO Substrate

NAME: Mr. Wanchai Deeloed

THIS THESIS HAS BEEN ACCEPTED BY

THESIS ADVISOR

(Assistant Professor Surachai Thachepan, Ph.D.)

THESIS CO-ADVISOR

(Assistant Professor Songwut Suramitr, Ph.D.)

DEPARTMENT HEAD

(Associate Professor Waraporn Parasuk, Dr.rer.nat.)

APPROVED BY THE GRADUATE SCHOOL ON _____

DEAN

(Associate Professor Gunjana Theeragool, D.Agr.)

THESIS

SYNTHESIS AND CHARACTERIZATION OF 1-D NANOSTRUCTURED TiO_2 ON FTO SUBSTRATE

WANCHAI DEELOED

A Thesis Submitted in Partial Fulfillment of
the Requirements for the Degree of
Master of Science (Chemistry)
Graduate School, Kasetsart University
2014

Wanchai Deeloed 2014: Synthesis and Characterization of 1-D Nanostructured TiO_2 on FTO Substrate. Master of Science (Chemistry), Major Field: Chemistry, Department of Chemistry. Thesis Advisor: Assistant Professor Surachai Thachepan, Ph.D. 86 pages.

Densely packed films of the nanosized TiO_2 crystals on Fluorine-doped Tin Oxide (FTO) glass substrate has been employed as the working electrode of the dye-sensitized solar cell (DSSC). Although the compact nanocrystalline TiO_2 film beneficially provides a large proportion of a specific surface area, the random pathway of electron in the film decreases device efficiency due to high possibility of the recombination of the charge carriers. Hence, this work focuses on a making of linear route for electron transportation by substituting the nanocrystalline film on the FTO substrate with the 1-D nanostructured TiO_2 film.

Two synthesis methods, template-assisted synthesis and hydrothermal synthesis, were employed in this study. The 1-D nanostructured TiO_2 on FTO substrate was successfully prepared by using the hydrothermal route in the presence of Cl^- ions. By using either the other types of substrate, Teflon and normal glass slide, or another specie of anion, SO_4^{2-}, the required nanostructure was not obtained. The crystallization of the 1-D nanostructured TiO_2 on the FTO substrate is believed to occur with the association of epitaxy relationship and surface roughness of substrate. This synthesis yielded the preferred oriented rutile TiO_2 nanorod film. This lead to the disappearance of both the (110) and (100) reflections of the TiO_2 in the XRD analysis.

The electrochemical impedance spectroscopy (EIS) was employed to investigate the electrical performance of the synthesized TiO_2 electrode and compared with the result obtained from the as-prepared nanocrystalline electrode. The comparison show that the 1-D nanostructured TiO_2 films have a lower charge-transfer resistance than the nanocrystalline film.

_____ _____ ___ /___ /___

Student's signature Thesis Advisor's signature

ACKNOWLEDGEMENTS

It is my pleasure to give my thankfulness to many important persons who have always been supporting me during my study at Kasetsart University. First of all, I would like to offer my heartfelt thanks to my great supervisor, Asst. Prof. Dr. Surachai Thachepan. He is the man who has never ever given up, in order to improve my scientific and moral thinking. More and more things have been given to me without asking for anything in return. Equally important, I am also thankful to my co-advisor, Asst. Prof. Dr. Songwut Suramitr, for his informative support and all his kind explanations. He always give me good guidance and vision that is very valuable.

I have been deeply indebted to my scholarship, the Development and Promotion of Science and Technology Talents Project (DPST), for the full-financial support during the time I have spent on my Bachelor and Master degrees. During the 7 years of study at Kasetsart University, many great experiences were provided to me by DPST. It is my honor to be one of the DPST students.

In addition, I wish to thank to my friends, the colleagues and all the staff in the department of chemistry at Kasetsart University. Moreover, special thanks go to all colleagues at the College of nanotechnology, King Mongkut's Institute of Technology Ladkrabang (KMITL) for all the help and experimental support.

Lastly, all my goodness should be attributed to all the guidance from my family. They have never ever left me alone and are always with me.

Wanchai Deeloed

June, 2014

TABLE OF CONTENTS

Page

LIST OF TABLES

LIST OF FIGURES

LIST OF FIGURES (Continued)

LIST OF FIGURES (Continued)

SYNTHESIS AND CHARACTERIZATION OF 1-D NANOSTRUCTURED TiO_2 ON FTO SUBSTRATE

INTRODUCTION

Invention of dye-sensitized solar cell (DSSC)

Nowadays, the demand for energy is increasing annually. The depletion of the supplied fossil fuel increased the cost to produce energy. Moreover, energy production through the combustion of fossil fuels emits carbon dioxide (CO_2), led to the problem of global warming, climate change, food production and starvation. Conversion of the solar power has been believed to be a promising way for the sustainable and clean energy production. Solar radiation can be directly converted to electricity through a photovoltaic (PV) devices widely known as solar cell. Today, the PV devices are commercially available on the market. However, the price of the PV devices are relatively high in comparison with the fossil-based fuel. Therefore, it is incompatible for many developing countries to base their energy supply on the solar power.

It is generally known that the major contribution of PV market shares is accounted on the Si-based solar cell, which is 80% of the total market shares (Zang, 2011). The raw material for Si-based solar cell is SiO_2 or sand, which is one of the most abundant substance found on the earth surface. The price of the PV panel mostly depends on the cost of pure Si production (Figure 1a) (Müller *et al.*, 2006 and Ranjan *et al.*, 2011). This process is still unoptimized due to the requirement of higher technology. Therefore, the invention of cost-effective solar cell is necessary. Dye-sensitized solar cell (DSSC) is an organic-inorganic hybrid solar cell. It has been invented by Brian O'regan and Michael Grätzel (O'Regan and Grätzel, 1991) to be a cost-effective device. The invention of this device has made a big impact on the research society. In the past two decades, the research on the area of DSSC development became increasingly more popular as evidenced by an increasing in the

annual research publication (Figure 1b). Until now, the researcher is still looking forward to improving their efficiency.

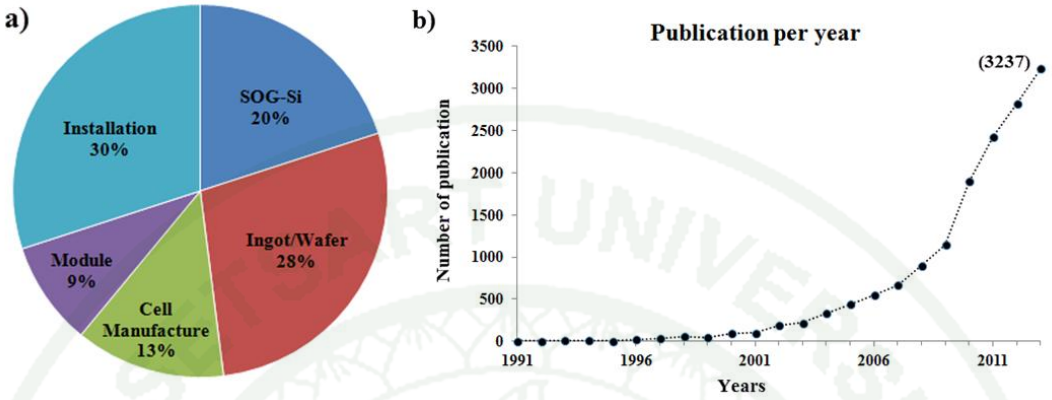

Figure 1 (a) A pie-chart showing approximate contribution in the production costs of Si-based solar module (adopted from Ranjan *et al.*, 2011). (b) The number of publications in the area of DSSC research from 1991 to 2013.

The concepts of the device making are based upon mimicking the photosynthesis of green plants. The light-absorbing molecule, chlorophyll, is a natural sensitizer that traps and converts solar radiation into chemical energy, stored as high energetic compounds, NADPH and ATP. It is complicated to discuss the change of chemicals in the photosynthesis. However, the process can be considered as the redox-reaction through the electron transport chain. In DSSC, the light-sensitive dye molecule with a good quantum yield is synthesized by the chemist in laboratory and used instead of the chlorophyll. The sensitized molecule is designed to absorb on mesoscopic metal oxide film of semiconductor which acts as a transport medium of electron. The photo-sensitive layer is coated on the transparent conductive oxide (TCO) glass (Figure 2). This is a photo-sensitized electrode, sometimes called working electrode or photo-anode. This electrode is used to assemble the DSSC with some additional components similar to the practical electrochemical cell. Three major components of the DSSC are described below,

Working electrode is consisted of porous semiconductor film containing photo-sensitive dye molecules. This layer is coated on the transparent conductive

oxide material (TCO) such as fluorine-doped tin oxide (FTO) glass. TiO_2 is a common oxide used in making this film. This electrode plays a big role in trapping solar radiation, energy conversion and electron transfer.

Counter electrode is usually made of Pt catalyst layer coated on the FTO glass.

Electrolyte typically used is a solution of iodide/tri-iodide redox couple (I^-/I_3^-) in dried acetonitrile. The redox couple system is very important to complete the electrical circuit in DSSC. The redox couple is also important in the regeneration of active dye-sensitized molecule.

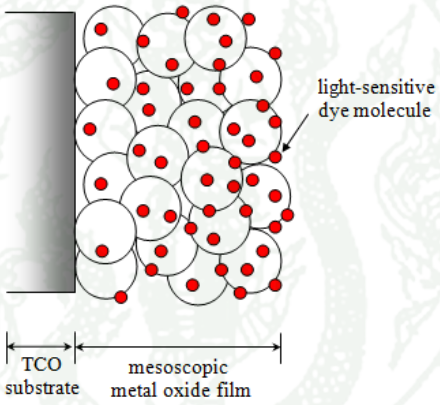

Figure 2 The illustration showing typical components in the working electrode of DSSC.

Operating principle of the photo-electrochemical cell is based on the three components as mentioned previously which are depicted in Figure 3.

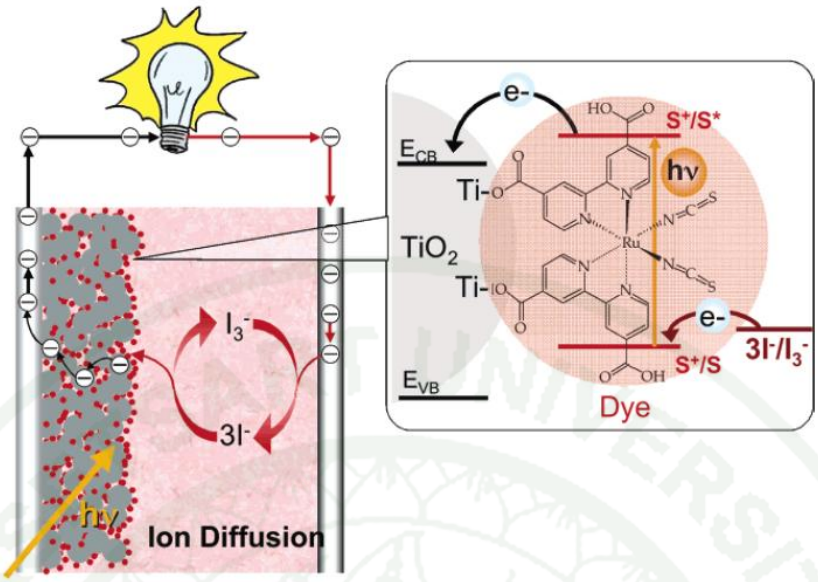

Figure 3 Illustration of the operating principle of DSSC.

Source: Grätzel (2005)

The cycle of energy conversion has been thoroughly explained (Grätzel, 2005; O'Regan and Grätzel, 1991 and Ramamurthy and Schanze, 2003). It starts via the stimulation of the sensitizer molecule (S) by sunlight. The sensitizer molecule in the porous semiconductor film is excited by absorption of energy from the sunlight (Eq. 1). The excited sensitizer (S^*) injects its electron into the conduction band (E_{CB}) of metal oxide through the transition process called metal-to-ligand charge transfer (MLCT). As a consequence, the oxidized dye (the sensitizer containing a positive charge, hole, S^+) and the negatively charged electron are formed in the porous oxide layer (Eq. 2). The injected electron flows through the porous oxide layer, the TCO, the external circuit and finally reaches the counter electrode. The electrolyte plays a crucial role in the recovery of the oxidized sensitizer to be the reduced form that is ready to perform the photo conversion again (Eq. 3). The redox couple can undergo self-regeneration by catching electron from the counter electrode (Eq. 4). The electron flows through the circuit, generating electrical current in the DSSC. This is the transformation of the solar energy to the kinetic energy of electron.

The cycle of energy conversion

$$S_{(\text{oxide surface})} + h\nu_{(\text{sunlight})} \rightarrow S^{*}_{(\text{oxide surface})} \quad \text{(Eq. 1)}$$

$$S^{*}_{(\text{oxide surface})} \rightarrow S^{+}_{(\text{oxide surface})} + e^{-}_{(\text{injected})} \quad \text{(Eq. 2)}$$

$$S^{+}_{(\text{oxide surface})} + \frac{3}{2} I^{-} \rightarrow S_{(\text{oxide surface})} + \frac{1}{2} I_3^{-} \quad \text{(Eq. 3)}$$

$$I_3^{-} + 2\, e^{-}_{(\text{cathode})} \rightarrow 3\, I^{-} \quad \text{(Eq. 4)}$$

The recombination process (competition reactions)

$$S^{+}_{(\text{oxide surface})} + e^{-}_{(\text{oxide surface})} \rightarrow S_{(\text{oxide surface})} \quad \text{(Eq. 5)}$$

$$I_3^{-} + 2\, e^{-}_{(\text{oxide surface})} \rightarrow 3\, I^{-} \quad \text{(Eq. 6)}$$

However, there are some undesirable reactions that can decrease the efficiency of the device. The excited molecule probably emit the consumed energy via fluorescent or thermal relaxation processes to come back to the ground state (the reverse reaction of Eq. 1), depending on the life time of the transition state. Moreover, the injected electron can recombine with either the oxidized dye or the redox electrolyte (Eq. 5 and 6). These widely known *recombination process* have become a serious obstacle for the DSSC development.

Titanium dioxide (TiO_2)

TiO_2 is a solid metal oxide possessing many forms of crystal structure. However, the three main phases that have been extensively studied are anatase, rutile and brookite.

The most stable phase of TiO_2 is rutile. It has been used as white pigment in industry such as household paint and cosmetic, due to its non-toxicity, high chemical stability and high reflective index. Rutile has been used medicinally in dermatology, bone regeneration and in semiconductor research (Brammer *et al.*, 2012 and Smith *et al.*, 2011). In photochemistry, rutile is used in the photo-induced electrochemical process such as the generation of the H_2 fuel by water oxidation (Zhang *et al.*, 2010).

Photochemical separation of electron-hole pair is used in the purification of waste water.

However, in the area of photocatalysis, another phase of TiO_2 has been reported to show a better performance than the rutile (Linsebigler *et al.*,1995). The second most stable phase of TiO_2 is anatase. The research on anatase is rapidly developed, especially in the area of photo-catalysis. Due to the high active area and low band gap of photo-excitation, anatase is widely used in the degradation of many contaminants in aqueous system. For example, anatase showed an excellent performance in the remediation of waste water from textile industries as a using of many commercial dyes such as methylene blue (MB), methyl orange (MO), methyl red (MR) and acid orange (AO) as the model compound to study (Neppolian *et al.*, 2002 and Wang *et al.*, 2004). Moreover, it has been reported that anatase shows an excellent bleaching power of the azo dye (Comparelli *et al.*, 2005; Dong *et al.*, 2010 and Liu *et al.*, 2006). Harmful species such as polycyclic aromatic hydrocarbon (PAHs) and arsenic have been reported to be remedied by the anatase (Dong *et al.*, 2010; Yao *et al.*, 2012 and Yoon *et al.*, 2005). Chemical doping with the other elements has been introduced to improve the performance of the anatase. Doping the anatase TiO_2 by anion dopants such as N, S and F and transition metal such as Ce, La, Eu and Sm have been reported (Wang *et al.*, 2000 and Wang *et al.*, 2006.)

The third known phase of TiO_2 is brookite. It has been reported in many studied that brookite is a byproduct during the phase transformation from anatase to rutile, implying the difficulty in producing large amount of brookite. However, there are some reports that show an efficient way to produce brookite with a high amount (Deng *et al.*, 2010 and Pottier *et al.*, 2001). The research on its application is relatively less extensive than rutile and anatase (Diebold, 2003).

Anatase and brookite are the metastable phases while the rutile is the most stable form of TiO_2. Transformation of crystal structure from the metastable phases to the stable one has often been achieved via the thermal treatment. Traditional way to yield the nanosized crystals of TiO_2 is the utilization of the sol-gel technique,

followed by calcination in air under high temperature. Anatase appears at the temperature about 450 ^{o}C and the threshold for rutile has been reported at 700 ^{o}C. In contrast, large amount of brookite has been synthesized by hydrothermal technique (Deng *et al.*, 2010 and Pottier *et al.*, 2001). Various methods in TiO_2 preparation are reported in the literature review.

In DSSC, TiO_2 is used to fabricate a porous oxide film in the working electrode. The porous network film of TiO_2 nanocrystal plays a crucial role in determining the DSSC efficiency, which can be attributed by two reasons below:

1. The porous network of TiO_2 nanocrystals provide a large proportion of specific surface area for the adhesion of sensitizer molecules. The higher the amount of dye loading the higher the photo-generated current. The most effective sensitizer is currently the complex of ruthenium (Ru). The ruthenium dyes available in the market are N719 and N3. The coordinated ligand in the Ru complex is usually terminated by the carboxylic end. This functional group preferably creates strong covalent bond with TiO_2 surface.

2. The porous layer of TiO_2 acts as a medium for the migration of electron from the excited sensitizer to the TCO layer. TiO_2 has been reported to show the highest injection rate of electron transfer from the lowest-unoccupied molecular orbital (LUMO) of the excited sensitizer to the conduction band.

Other oxides such as ZnO and SnO_2 are also used in DSSC (Manthina *et al.*, 2012, Shang *et al.*, 2012 and 2013). However, the most popular is TiO_2. In addition, bare TiO_2 on TCO substrate can be used as an electrode in the other application. For example, TiO_2 electrode has been used to sense the UV radiation and many organic compound (Cao *et al.*, 2011 and Mu *et al.*, 2011). TiO_2 has been used as photo-electrode in the photo-electrochemical water splitting (Maeda and Domen, 2010).

Background of study, proposed solution

The traditional TiO_2 photo-electrode has been prepared by doctor blade technique using commercial colloidal dispersion of TiO_2 nanocrystals. The dispersion was painted on the TCO substrate, followed by the heat treatment. The prepared TiO_2 electrode was immersed in a solution of sensitizer to allow the chemi-sorption of the sensitizer onto the porous network. The DSSC prepared from this electrode has been reported to show more than 10% of solar conversion efficiency (Grätzel ,2005). However, many research groups have tried to improve the efficiency by organizing the nanostructure of TiO_2 film (Thavasi *et al.*, 2009 and Zhang and Cao, 2011). The key consideration for making the efficient photo-electrode has been proposed as followed,

1. The efficient photo-electrode should have high specific surface area in order to maximize the dye loading amount. In this regard, nanocrystalline TiO_2 film responses very well. However, the high specific surface area also provides more number of active sites for the recombination at the same time.

2. The efficient photo-electrode should possess low connective site of grain boundary. The porous network of nanocrystalline film generates tremendous connective sites in the film. The connecting site in the network acts as the energy barrier which traps electron to remain in the boundary (Figure 4). The trapping event promotes the possibility of recombination process. Therefore, the connective sites should be minimized.

3. The efficient photo-electrode should serve the linear pathway of electron transfer. The colloidal TiO_2 film gives the random route of electron migration (Figure 5a) that increases the possibility of recombination between electron and oxidized species. The problems may be solved by providing the 1-D nanostructure to this system (Figure 5b).

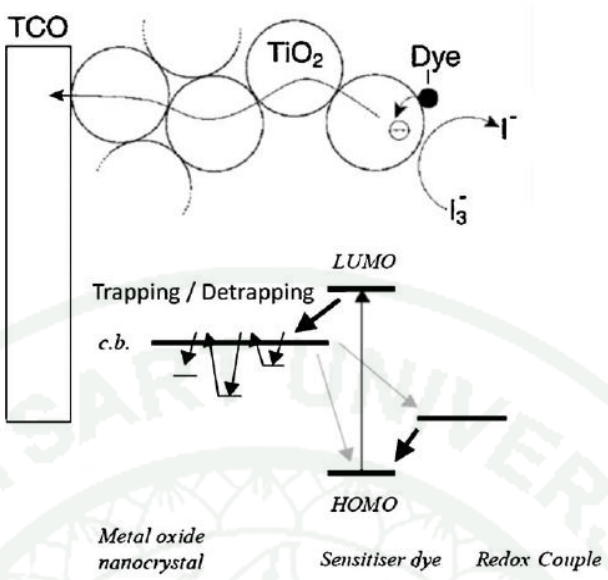

Figure 4 The diagram of electron transportation in colloidal TiO_2 film. Electron can be trapped at the grain boundary of TiO_2 nanocrystal.

Source : Zhang and Cao (2011)

Figure 5 The diagrams of electron mobilization in TiO_2 medium. a) a random pathway in the colloidal film. b) a direct pathway in the 1-D nanostructured TiO_2 film.

Source : Thavasi *et al.* (2009)

The colloidal TiO_2 film on TCO should be substituted with the 1-D nanostructured TiO_2. Therefore, synthesis of the 1-D nanostructured TiO_2 on the TCO substrate, using FTO as a model substrate, was the main objective of this study. Electrical performance of the synthesized TiO_2 electrode was investigated and compared with the standard colloidal TiO_2 electrodes.

OBJECTIVES

1. To synthesize 1-D nanostructured TiO_2 vertically aligned on FTO substrate

2. To study the effect of TiO_2 nanostructure on electrical property of the electrode

LITERATURE REVIEW

1. Review of general method to synthesize TiO_2

Acosta showed the preparation of TiO_2 thin film on the surface of glass and FTO by using two different method (Acosta *et al.*, 2005). The first technique was the DC reactive magnetron sputtering. The experiments were performed in the pre-vacuum chamber using a mixed gas (50:50, O_2 to Ar ratio) with varying the pressure (4, 8, 16 and 32 mtorr). The metal target was the pure Titanium, placed above target substrate for 5 cm. The second technique was the spray pyrolysis method. The mixture of 0.08M $TiO[C_5H_7O_2]_2$ in alcoholic solution (100 cc. ethanol and 5 cc. HCl) was sprayed on the heated substrate (300 ^oC, 350 ^oC, 400 ^oC and 500 ^oC). Pure air was used as a transport gas. Product from both method occurred in a form of poly-crystalline TiO_2 film. The anatase phase was reported to be major product from the both process. However, rutile became the main proportion in some condition.

Zhou reported the preparation of the mesoporous TiO_2 microsphere by hydrothermal technique (Zhou *et al.*, 2010). The $Ti(SO_4)_2$ was used in the experiment as a sole Ti source and dissolved in urea ($CO(NH_2)_2$) aqueous solution. The molar ratio of urea to Ti source was constantly kept for 2. The solution was sealed in the Teflon-liner stainless steel autoclave. Hydrothermal reaction was carried out at 160 ^oC with the variation of time (1, 3, 5, 7 and 12). Product appeared as a microsphere TiO_2. N_2 sorption, SEM and TEM results demonstrated that the microsphere possessed the mesoporous structure, due to the aggregation of nanosized TiO_2 crystals. The aggregation was explained by minimizing total surface energy of the system. This method showed an advantage to produce pure phase of TiO_2 at low temperature without any further heat-treatment.

Deng reported the route to selectively produce rutile, anatase and brookite TiO_2 from titanate nanosheet (Deng *et al.*, 2010). Hydrothermal synthesis was employed as the synthesis method. They found the way to selectively produce pure phase of TiO_2 was achieved by tuning the pH of the precursor solution. The result

indicated that the formation of rutile favored the very high acidic condition (above pH = 0), while the pH raging from 1 to 11 was favored for anatase formation. Moreover, pH ranging from 9 to 11 was appropriated for the formation of brookite. Characterization by XRD confirmed the high purity of products. The dissolving-recrystallization-growing mechanism has been proposed to describe the results.

2. Review of the method to synthesize the 1-D nanostructured TiO_2

The using of hard template was thoroughly reviewed as a one of straightforward route to produce many kinds of the 1-D shape such as nanorod, nanotube and nanowire (Cao and Liu, 2008). Growing of nanotube (or rod) diameter, length and wall thickness were independent and seemed to be controlled through some factors such as concentration, temperature, time and current. Template-assisted method was separated to four different types. The first type was the electrochemical deposition that referred to the growth of the reactive charged species which were able to move under the external-applied electric field. This method was suitable to grow the 1-D shape metals, alloys, semiconductors and other electrically conductive materials. Electrophoretic deposition was the second route which were different by using of dielectric materials. Growing of the 1-D single-crystalline metal oxide from colloidal suspension was realized by this method. The third method was the template-filling method that more common than the others. Filling the void of template by precursor solution, followed by heating and template etching was the direct route to yield the 1-D nanostructure. Finally, converting of reactive templates was the last method. The reactive backbone was prepared prior to the deposition of the desired chemicals on their surface. Then, the template was removed to leave the desired material in the same morphology. However, this method was not resulted in the array of the 1-D products. This method was usually employed to produce complex nanostructure such as the urchin-like nanoflower that was built from a number of the nanotube spines.

The heating sol-gel template method was employed to produce the array of TiO_2 nanorod (Miao *et al.*, 2004). The technique was composed of two components, template and Ti-sol solution. The porous anodic aluminar membrane (AAM) was employed as a template which was pre-treated by soaking in boiled ethanol for10 minute and dried for 24 hrs in ambient condition. The TiO_2 sol solution was made by typical sol-gel technique. The Ti-sol solution was prepared by the mixing of Ti(IV) isopropoxide, acetyl acetone, de-ionized water and ethanol in the molar ratio at 1:1:3:20. Then, the AAM template was immersed in the boiled sol solution (80 ^oC). The AAM template was infiltrated by the Ti-sol and dried for one day. The occupied template was annealed in the muffle furnace with the designed program of heating rate and time. Finally, the array of TiO_2 nanorods was obtained by performing the chemical etching of template. TEM result confirmed that the as prepared nanorod was the poly-crystalline 1-D nanorod. The results indicated that the structure of TiO_2 in nanorod could be directly controlled via the calcined temperature. The anatase phase was produced from 400 ^oC of annealed temperature, while the rutile was achieved at 700 ^oC. This method showed the convenient way in the controlling of size and shape of nanorod. The aspect ratio of nanorod can be directly tuned via using the appropriate void of template.

The preparation of TiO_2 nanotube array on metallic substrate by electrochemical technique was reported by Lin (Lin *et al.*, 2011). The TiO_2 nanotube array occurred from the anodization of Ti foil in the ethylene glycol solution containing 0.5% w.t. NH_4F and 3% de-ionized water at a constant voltage. The film was subsequently heated and electrochemically self-detached from the Ti foil to obtain the free-standing film of TiO_2 nanotube array. The free-standing film was adhere on FTO substrate by using the TiO_2 nanoparticle paste and followed with the sintering at 450 ^oC for 3hrs. The adhered sample was sensitized with a commercial dye to make the photo-electrode in DSSC and tested the performance. Moreover, a variety of different-morphology free-standing nanorod film was prepared by the same technique, and also used as the photo-electrodes. The synthesized nanotube photoelectrode was reported to show the higher performance than the DSSC made from the nanoparticle photoelectrode.

3. Reviewed of nanoparticle based electrode in DSSC

Because Lithium-containing electrolyte was widely used in DSSC, the effect of Li intercalation in TiO_2 nanocrystalline film was studied (Kopidakis et al., 2003). The nanocrystalline TiO_2 film was prepared on the FTO glass by conventional doctor blade casting technique and electrochemically doped by Li with the atomic density less than 5%. They found that it was the first evidence that electron transportation limited the recombination with the redox electrolyte in the working electrode. They found that the higher percentage of intercalation Li led to the slower of both charge transportation and recombination. They concluded that recombination in DSSC was the diffusion-limited process, and conclude that it was worth nothing to enhance the performance of DSSC through the increasing of diffusion rate of nanocrystalline film.

Contrasting the performance between rutile and anatase in making the DSSC was performed (Park *et al.*, 2000). Nanocrystalline TiO_2 electrode was prepared by varying the crystal structure of TiO_2 as two types, rutile and anatase. Those nanocrystalline electrode was used to fabricate DSSC and compared their performance. They reported that the working electrode DSSC made from the nanocrystalline rutile TiO_2 exhibited the conversion efficiency of about 5.6%, while the better result was given form the using of anatase phase, about 7.1%. They explained that the better result of anatase risen from 2 factors, the higher surface area per unit volume and the higher electron transportation. The result from SEM was the crucial evidence to approximate the surface area per unit volume of nanocrystalline electrode. The rutile electrode was approximated to possess the lower surface area than the anatase electrode for 25%. The result from photosensitization experiment agree well with the conclusion. The significant role of the second factor was confirmed by IMPS study. They found that the nanocrystalline rutile film had the lower effective electron diffusion coefficient (D_{eff}) that anatase film about an order of magnitude, at the same measured J_{sc}.

4. Review of electron mobility in the nanoparticle based electrode

Ansari-Rad showed the computational study of one electron diffusion in the simulated nanocrystalline film by Monte-Carlo random walk simulation (Ansari-Rad *et al.*, 2011). The nanocrystalline film was constructed base on the nanosized sphere which represented the nanosized crystal in TiO_2 film. The sphere was varied with the radius in the range of $10 < r < 18$ nm. Trapping state in the system was either the surface defect or the volume defect of nanoparticle. Porosity of the simulated mesoporous film was varied by tuning the overlapping fraction. They reported that the appropriate range of film porosity should be between 44-52 %, whereas the real value was 50-60%. They found that the diffusion coefficient of electron in the film was independence from film roughness. However, according to the result obtained at a constant photocharge density, effect of film roughness on the surface diffusion was observed. They reported that porosity of the film is an important parameter to determine both surface diffusion and volume diffusion of electron in the mesoporous film.

Electron transportation in the nanocrystalline ZnO layer on the ITO substrate was study (Noack *et al.*, 2002). Nanocrystalline ZnO film on the ITO substrate was prepared by spin coating the suspension of ZnO nanoparticles in ethanol on the substrate with subsequently annealed. Electrochemical study of the electrode showed that transient photo-current, $i(t)$, was composed of three component as the equation, $i(t) = i_I(t) + i_D(t) + i_T(t)$, which were ascribed to the three different charge transfer processes, fast initial charge transport, slow transport via deep trap state and the transport via the conduction band state (shallow traps). According to the result the transfer through the conduction band, $i_D(t)$, seemed to be the key process of transport phenomena in ZnO/ITO electrode. They also proposed the mathematic equation to predict the transport model with a good agreement with the experimental results. They found that the measured current should be attributed to the transport processes in the ITO and ZnO layer. The fast risen transient current should be ascribed to the transport in ZnO layer due to the diffusion through the shallow trap state, whereas the slow decay was determined by the diffusion in ITO substrate. They concluded that charge

transfer through ITO and equipment connection limited the transportation rate. The results indicated that, after the excitation, the photo-generated charge was rapidly accumulated at the inter-region of nanocrystalline ZnO layer and the ITO surface in comparison with the discharge process performed in ITO layer.

A comparison study of TiO_2 nanofiber and nanoparticle was investigated by Choi (Choi *et al.*, 2010). The nanofiber was prepared by electrospinning of TiO_2 powder dispersed in viscose polymer solution, followed by calcination. The nanoparticle was generated to compare with the former by the same method excluded the spinning step. General characterization found that TiO_2 resulted in a form of polycrystalline anatase. Nanofiber with the diameter about 500 nm was successfully prepared. N_2 adsorption-desorption experiment showed type IV isotherm and H3 hysteresis loop from both samples, indicated the mesoporosity. However, BJH pore size analysis showed that TiO_2-NF possessed the twice specific surface area of nanoparticle. It could be implied to the increasing of porosity during the electrospinning process and interspacing by the polymer. Photocatalytic study found that the nanofiber exhibited the higher photocurrent than the nanoparticle by a factor of 3, and the performance of H_2 production was also higher by a factor of 7. The higher performance should be ascribed to the larger specific area and the better of separation and transfer of photo-generated charge.

5. Review of using the 1-D nanostructured TiO_2 to enhance electrical properties

Mixing of the TiO_2 nanotube with TiO_2 nanoparticle has been reported to show the enhancement of DSSC efficiency (Zhong *et al.*, 2011). TiO_2 nanotubes was prepared by electrochemical anodization of Ti sheet. The result product was blend with TiO_2 nanoparticles with the varying concentration of nanotube and used to fabricated the DSSC. EIS and OCVD study revealed that increasing the nanotubes proportion could enhance both lift time and transportation of electron, while the diffusion length was dramatically decreased. The 10% wt. of nanotubes was reported to show the best performance, 3.11%, due to the fact that a large proportion of nanoparticle served the high loading amount of sensitizer molecule. However, the

higher the degree of nanotube resulting in the lower of specific surface area. Moreover, they proposed that the exceed amount of nanotubes, more than 10% wt. of nanotube, would create the dead loop of electron transportation.

Yi had been developed the flexible gas sensor by using the incorporation between the one-dimension ZnO nanorod and the free-standing graphene-metal sheet (Yi *et al.*, 2011). Typically, the ZnO nanorod was hydrothermally grown on the stainless steel foil pre-grown by the 200 nm thick ZnO seeding layer using MOCVD method. The graphene sheet was grafted on the $Si/SiO_2/Ni$ substrate by the chemical vapor deposition method (CVD), and then subsequently coated with Au and poly(methyl metacrylate) (PMMA). Free-standing graphene/Au/PMMA was obtained after the chemical etching of the Si/SiO_2 and Ni layer with HF and TFG Ni etchant, respectively. Then, the graphene/Au/PMMA was mounted on the ZnO nanorod, and finally, removed the PMMA layer by oxygen plasma to obtain the hybrid gas-sensor. They reported that the device can detected the ethanol vapor in the level of ppm. Moreover, this device maintained a constant performance without any significant loose of physical properties after repeating the bending-unbending process of the device for 100 times.

Electron transport in TiO_2 nanotube was study (Hsiao *et al.*, 2011). The anatase TiO_2 nanotube array was produced by anodization of Ti sheet in a solution of NH_4F in ethylene glycol and calcined at 450 ^oC for 30 minutes. The array was detached from the metal sheet via chemical etching. The nanotube array was employed to prepare DSSC. They found that the performance of DSSC was depended on the illumination methods they employed, the frontside illumination and the back-side illumination. They reported that the higher conversion efficiency of DSSC was resulted from the experiment performed by irradiate the device in the frontside. The investigation by using IMPS revealed that the photo current from the frontside illumination was composed of two components ascribing to the gemini process, trap-free diffusion and trap-limited diffusion process. They mentioned that trap state was referred to the crystal defect that remained at the grain boundary. The trap-limited diffusion was determined as the diffusion of electron generated at a far side from the

FTO substrate. The photo-generated charge had to diffuse along the tube, passed through many trap states at the grain boundary. Therefore, they were more likely to trap. On the contrary, the trap-free diffusion was referred to the photo-generated charge that was produced near the FTO. The photo-generated charge were freely passed through the trap state because traps were pre-occupied by the electron from the previous process. They both were the thickness-dependence diffusion. The 30 μm thick nanotube array seems to be the appropriate thickness to prepare the DSSC with the best performance. On the other hand, IMPS study of the back-side irradiated experiment showed that this mode resulted in only the trap-limited diffusion in the array. Backside illumination resulted in the longer electron lifetime. However, the different of lifetime seems to be non-significant to the transit time.

MATERIALS AND METHODS

In this work, both "template-assisted method" and "hydrothermal method" were employed to make the 1-D nanostructured TiO_2 on FTO substrate. Typically, hydrothermal synthesis yielded the TiO_2 in the form of nanorod, while the template-assisted method produced the nanotube (Miao *et al.*, 2004 and Liu and Aydil, 2009). Based on our experience, hydrothermal method provide more challenge than the template method. Hence, the synthesis of the promising electrode was mainly performed by following the hydrothermal route.

Materials

1. Acetone (C_3H_6O) : analytical grade, Carlo Erba
2. Acetyl acetone ($C_5H_8O_2$) : analytical grade, Fluka
3. Anhydrous sodium sulfate (Na_2SO_4) : laboratory grade (99.9%), Carlo Erba
4. Anodic Alumina Oxide template (Al_2O_3) : 13 mm. Anodisc circle, Whatman
5. Concentrated hydrochloric acid (HCl) : 37% w/w, Carlo Erba
6. Concentrated sulfuric acid (H_2SO_4) : 98% w/w, Carlo Erba
7. Ethanol (C_2H_5OH) : analytical grade, Carlo Erba
8. Fluorine-doped tin oxide (FTO) coated glass substrate : Solaronix SA
9. Iso-propanol (C_3H_7OH) : analytical grade, Scharlau
10. Laboratory glass slides
11. Methanol (CH_3OH) : analytical grade, Carlo Erba
12. Titanium(IV) isopropoxide ($C_{12}H_{28}O_4Ti$) : laboratory grade (98+%), Acros organics
13. Titanium dioxide paste (TiO_2) : PST-18NR, JGC Catalysts and Chemicals Ltd.
14. Titanium dioxide nanopowder (TiO_2) : laboratory grade (99.9%), Sigma-Aldrich
15. Triton X-100 ($C_{14}H_{22}O(C_2H_4O)_n$) : laboratory grade, Fluka

Methods

1. Preparation of 1-D nanostructured TiO_2 by template-assisted method

1.1 Preparation of Ti-sol dispersion

In this work, the sol-gel synthesis was used to prepare Ti-sol dispersion (Miao *et al.*, 2004). De-ionized water (DI water) was used in the synthesis. Typically, 0.067 ml of DI water, 0.128 ml of acetyl acetone (ACAC) and 1.910 ml of iso-propanol (i-Pro) were mixed in a closed glass vial and stirred at 400 rpm. Finally, 0.370 ml of TTIP was added and the resulted mixture was continually stirred for 30 minutes to obtain the dispersion named TAPW - 11203. The solid content of Ti-sol dispersion was maximized by varying the mole ratio of reactants in the dispersion (Table 1). Four capital letters, T, A, P and W were used to symbolize the TTIP, ACAC, i-Pro and DI water, and four digit numbers were assigned to refer mole ratio of reactants, in the dispersion, one by one, respectively.

Table 1 Summary of the as prepared Ti-sol dispersions and compositions

Ti-sol dispersions	The amount of reactants in dispersion (ml)				mole ratio (T:A:P:W)
	TTIP	ACAC	i-Pro	DI water	
TAPW - 11203 (Miao et. al., 2004)	0.370	0.128	1.910	0.067	1 : 1 : 20 : 3
TAPW - 1153	0.370	0.128	0.478	0.067	1 : 1 : 5 : 3
TAPW - 1113	0.370	0.128	0.096	0.067	1 : 1 : 1 : 3
TAPW - 4153	1.480	0.128	0.478	0.067	4 : 1 : 5 : 3
TAPW - 1100	0.370	0.128	-	-	1 : 1 : 0 : 0
TAPW - 2100	0.740	0.128	-	-	2 : 1 : 0 : 0
TAPW - 4100	1.480	0.128	-	-	4 : 1 : 0 : 0

Three Ti-sol dispersions, TAPW - 4100, TAPW - 1113 and TAPW - 11203, and the fourth dispersion named "TAPW - 11203 (70 ^{o}C)" were chosen to synthesize the 1-D nanostructured TiO_2 via template-assisted method. TAPW - 11203 (70 ^{o}C) was produced by heating the TAPW - 11203 up to 70 ^{o}C during the template infiltration.

1.2 Infiltration of Ti-sol into the AAO templates

Anodic alumina oxide (AAO) template was employed as a template in this synthesis method. Firstly, pre-treatment is necessary in order to degrease the template surface. AAO template was cleaned by soaking in hot ethanol (70 ^{o}C) for 5 minutes and drying in ambient condition. After that infiltration of Ti-sol was carried out by either the following; the pre-treated AAO template was immersed into the Ti-sol dispersion for 5 minutes and dried in air or the pre-treated template was placed on a few drops of the dispersion on a glass slide. The infiltrated template was cured at 70 ^{o}C for 30 minutes, followed by sintering in muffle furnace (Nabertherm B180) at 450 ^{o}C for 5 hours.

1.3 Chemical etching of AAO template

The calcined sample was immersed in 10% w/v NaOH solution for 24 hours to digest the AAO template. The remaining product was washed by DI water until the washed liquor become neutral, and dried on a cleaned glass slide in air.

1.4 Characterization

Scanning electron microscope (SEM; JEOL JSM-5410, 20 kV equipped with elemental analyzer, Oxford INCA 300) and cold field emission scanning electron microscope (FE-SEM; JEOL JSM-6301F, 20 kV equipped with the elemental analyzer, Oxford INCA 350) were used to investigate morphology and elemental composition of the existing products. Product before chemical etching was investigate in a side view. It was cut and adhered to the side wall of metallic stub with the cutting

face upward using the carbon conductive adhesive tape. Product after the chemical etching, which were dried on glass slide, was prepared for SEM by placing the glass slide including them on the stub covered by the carbon tape. SEM samples were coated with Au to enhance conductive property of sample surface.

2. Preparation of 1-D nanostructured TiO_2 electrode by hydrothermal method

2.1 Preparation of Ti precursor solution

Preparation of Ti precursor solution was adapted from the method reported previously (Liu and Aydil, 2009). De-ionized water (DI water) was used in the synthesis. Ti precursor solution was freshly prepared before used in all hydrothermal syntheses. Briefly, 0.800 ml of Titanium(IV) isopropoxide (TTIP) was added to a mixture of 20.0 ml of de-ionized water (DI water) and 20.0 ml of conc.HCl with a continuous stirring at 350 rpm. The resulted solution was stirred for an additional 5 minutes or until a clear and colorless solution was obtained. The amount of TTIP in the 40 ml acidic mixture was varied as 0.800 ml, 0.600 ml, 0.400 ml and 0.200 ml to obtain the growth solutions named T_0.8, T_0.6, T_0.4 and T_0.2, respectively. Moreover, to study the effect of anion on structure and morphology of TiO_2, 2 M H_2SO_2 was used instead of HCl for a comparison.

2.2 Preparation of FTO glass substrates

FTO glass substrate was used in this work. It was cut with a diamond head glass cutter into the size of 1.50 cm ×1.00 cm and cleaned before used. Pre-treatment was done by immersing the substrates in a mixture of DI water, methanol and acetone (1:1:1 by volume) with a sonication for 15 minutes. The treated substrate was repeatedly rinsed with DI water. Normal glass slide was used for a control substrate and similarly prepared as the FTO.

2.3 Hydrothermal synthesis

Hydrothermal synthesis was performed in a 125 ml acid digestion vessel (Parr instrument company). Typically, the pre-treated substrates were placed on a teflon-liner either horizontally with the conductive side upward or vertically. After that, the Ti precursor solution was gradually poured to the level that covered the substrates surface. The teflon-liner was sealed in the stainless steel jacket and heated in an electric oven to the designed temperature (120 - 180 ^{o}C) for 6 hours and naturally cooled down to room temperature in fume-hood. Note that, typical condition was the synthesis at 180 ^{o}C with the using of 40 ml T_0.8 solution. The substrates were collected, rinsed with DI water for several times until the washed liquor become neutral, and dried in air.

2.4 Characterization

The scanning electron microscope (SEM; JEOL JSM-5410, 20 kV equipped with the elemental analyzer, FEI Quanta 450) and the cold field emission scanning electron microscope (FE-SEM; JEOL JSM-6301F, 20 kV equipped with the elemental analyzer, Oxford INCA 350) were used to investigate morphology of the synthesized TiO_2 film on the FTO substrate. Top view sample was prepared by placing the synthesized product on the metallic stub that covered with the carbon conductive adhesive tape. Cross-sectional sample was prepared by cutting the synthesized product by diamond head glass cutter. The result was adhered on the side wall of metallic stub by the carbon tape with the cutting face upwards. SEM samples were coated with Au (POLARON RANGE SC 7620, 10 mA, 120 sec.) to enhance electrical conductivity of sample surface. Analysis of SEM image was carried out by using image analysis program, ImageJ (version 1.46r).

Crystal structures of TiO_2 and substrate were investigated by X-ray diffraction technique (XRD; Bruker D8 ADVANCE A25, 40 kV). XRD analysis was performed from 20^{o} to 80^{o} using the Cu-K_{α} radiation (λ = 1.5406 Å), 0.01 mm Ni slit, 5.8 mm detector aperture, 0.8 minutes of data collection time and 0.020^{o} data interval.

XRD sample were either the TiO_2 film on substrate or the TiO_2 powder scratched from the FTO surface. The scratched powder was ground, spread on sample holder and smoothed down the surface before analyzed.

Transmission electron microscope (TEM; Hitashi HT 7700, 120 kV) and selected-area electron diffraction (SEAD) were performed to investigate growth behavior of the TiO_2 crystal. TEM sample was the TiO_2 crystals which mechanically scratched from the FTO surface. It was ground and dispersed in ethanol by sonication. The dispersion of TiO_2 crystal was dropped on the homemade carbon-coated Cu grid (400 mesh) and dried in air.

Electrochemical impedance spectroscopy (EIS) was performed to study the resistivity of the synthesized 1-D nanostructured TiO_2 film. The experiment was performed in the Potentiostat/Galvanostat (Methrohm, AUTOLAB-PGSTAT 302N). The investigation was performed in the frequency range of 0.05 Hz - 100 kHz by using 0.1 M Na_2SO_4 aqueous solution as an electrolyte. The Ag/AgCl and Pt electrodes were employed as the reference and counter electrode, respectively. The 1-D nanostructured TiO_2 electrodes named NR-T_0.8, NR-T_0.6 and NR-T_0.4, were synthesized from T_0.8, T_0.6 and T_0.4, solitions, respectively. They were used as the working electrode with the fixed area of 0.5 cm × 0.5 cm of TiO_2 film, prepared by mechanical scratching. The FTO surface was partially covered by the normal adhesive tape to produce the exposed area of 0.2 cm × 1.0 cm the ohmic contact. EIS results were analyzed by using NOVA program (version 1.10.3).

Two nanoparticle-based electrodes, P25 and P25_900, were measured for comparison (Table 2). P25 electrode was the thin compact layer of nanocrystalline TiO_2 on FTO substrate, made from the commercial grade colloidal paste of anatase TiO_2. P25_900 electrode was similar electrode as the previous one, however, prepared from the homemade colloidal paste of rutile TiO_2 nanocrystals. The rutile nanocrystal paste was prepared by mixing the rutile nanopowder with the binder, triton X-100. Rutile TiO_2 powder was obtained by sintering the commercial TiO_2 powder (P25) at 900 ^oC in air for 6 hours. The compact layer of TiO_2 nanoparticles on the FTO was

prepared by the conventional method called "Doctor blade technique". Typically, nanoparticle paste was spread on the cleaned FTO substrate with the area of 0.5 cm × 0.5 cm using the adhesive tape as a template. After the removing of template, the paste on the FTO was cured at 100 ^{o}C for 15 minutes, and followed by the calcination in air at 450 ^{o}C for 3 hours. The exposed FTO surface was covered using similar condition as the 1-D nanostructured TiO_2 electrode. All EIS samples in this study were summarized in Table 2.

Table 2 Summary of TiO_2 electrodes in the EIS experiment.

Electrodes	**TiO_2 film's morphology**	**Crystal structure of TiO_2**
NR-T_0.8	The vertical array of TiO_2 nanorods on FTO substrate	Rutile
NR-T_0.6		
NR-T_0.4		
P25	The compact layer of TiO_2 nanoparticles on FTO substrate	Anatase
P25_900		Rutile

RESULTS AND DISCUSSION

1. Synthesis of 1-D nanostructured TiO_2 by template-assisted method

Preparation of Ti-sol dispersion was carried out by using the traditional sol-gel synthesis method. The prepared dispersion mostly appeared as the clear yellow to orange liquid, excepted the dispersion named TAPW-1100 and TAPW-4153 which solidified after 45 minutes of stirring. After performing the infiltration of template by the chosen Ti-sol dispersions and sintering, the 1-D nanostructure was produced (Figure 6). Typically, top side of AAO template were covered by thin film, whereas the void in the template was fulfilled with the solid substance. The results were differed from the SEM images of the bared AAO template shown in Figure 7. However, significant difference from the varying of solid content in dispersion was not observed in this work.

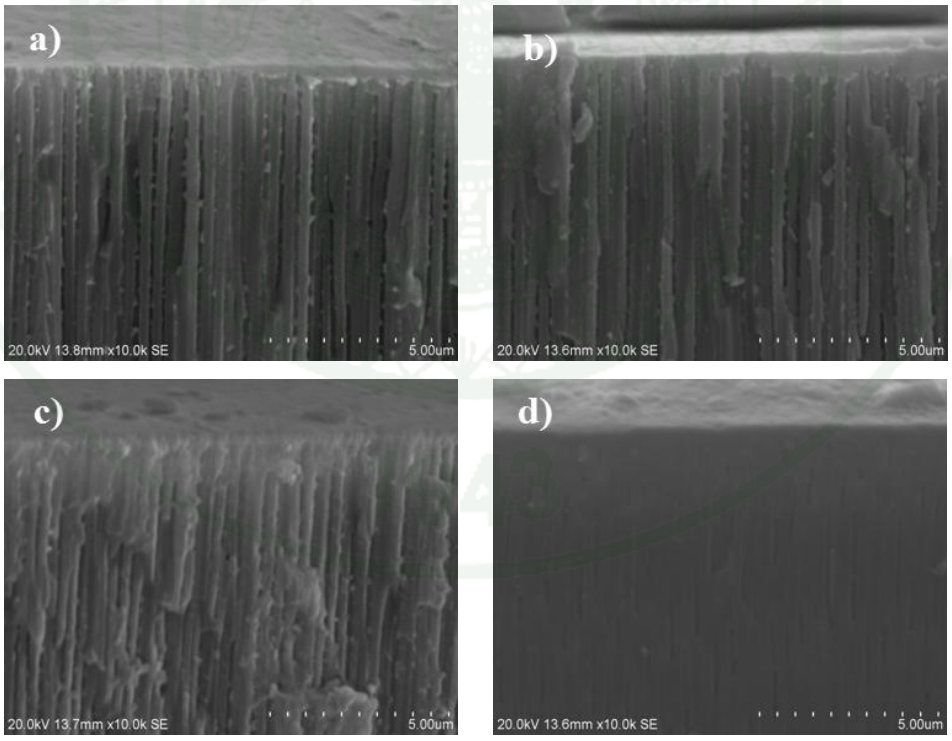

Figure 6 SEM images of the AAO templates fulfilled with 1-D nanostructured products synthesized from the dispersion named (a) TAPW - 4100 (b) TAPW - 1113 (c) TAPW - 11203 and (d) TAPW - 11203 (70^{o}C).

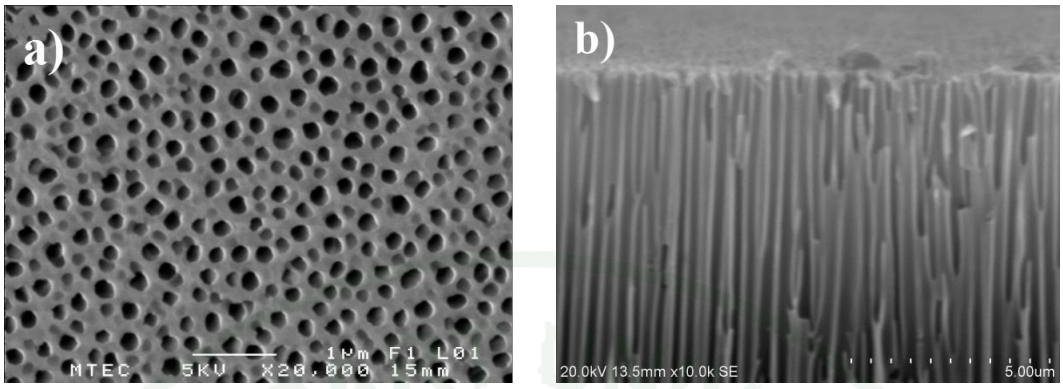

Figure 7 SEM images of the bared AAO template; (a) a top view and (b) a side view.

Chemical etching of AAO template was carried out by using the 10% w/v NaOH aqueous solution. Figure 8 showed EDS analysis of products, obtained after performing the chemical etching, of those synthesized from TAPW - 1113. Two different morphology solids was observed in the sample, indicated by a small box in the inset a and b.

Analysis of the indicated area in the inset a showed a large proportion of O, Na, Al and Si. The existence of Si in the diagram could be subjected to the glass substrate which was used as a support in the preparation of SEM sample. The presence of Na and Al should be referred to the residue which still remained after the chemical etching of template.

In contrast, the investigation on the indicated area in inset b showed a large proportion of Ti which could be account for the 1-D nanostructure and some trace of Al, Na and Si. The result confirmed that the etching process was uncompleted that led to the existence of flake solid and some existence were also remained in the nanostructure.

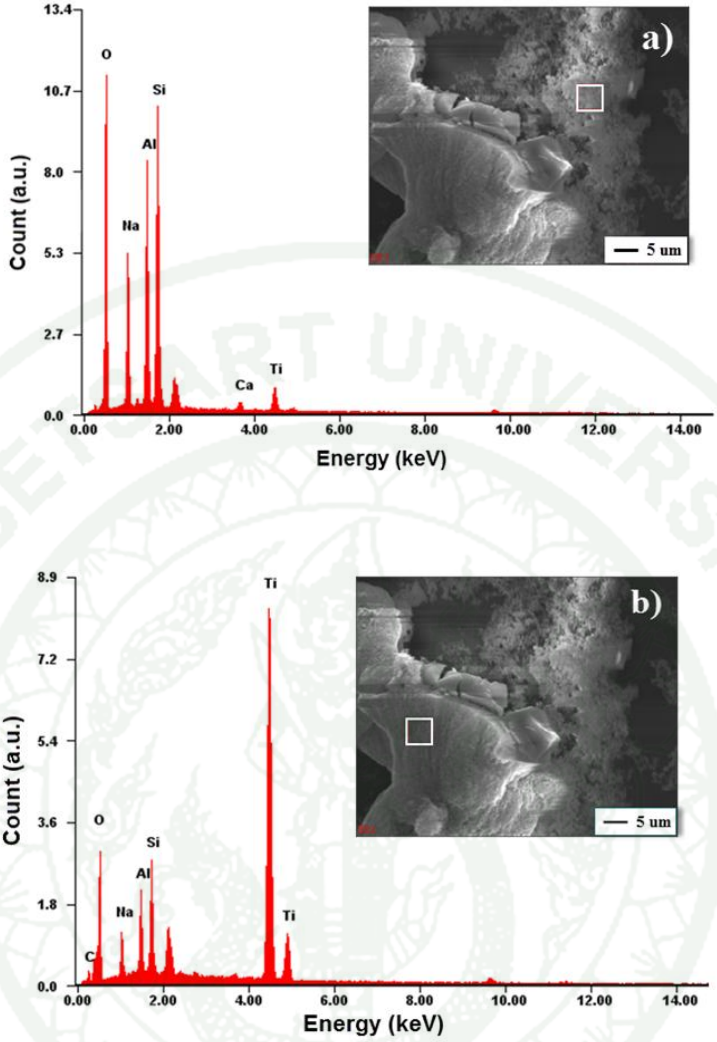

Figure 8 Elemental analysis of products after chemical etching. The sample was synthesized from the TAPW - 1113 dispersion. Investigation area was indicated in the inset by a square box.

SEM images of the synthesized 1-D nanostructured TiO_2 from all employed dispersion were shown in Figure 9. The result was obtained in the form of nanorod array that seemed to be similar to the shape of template void.

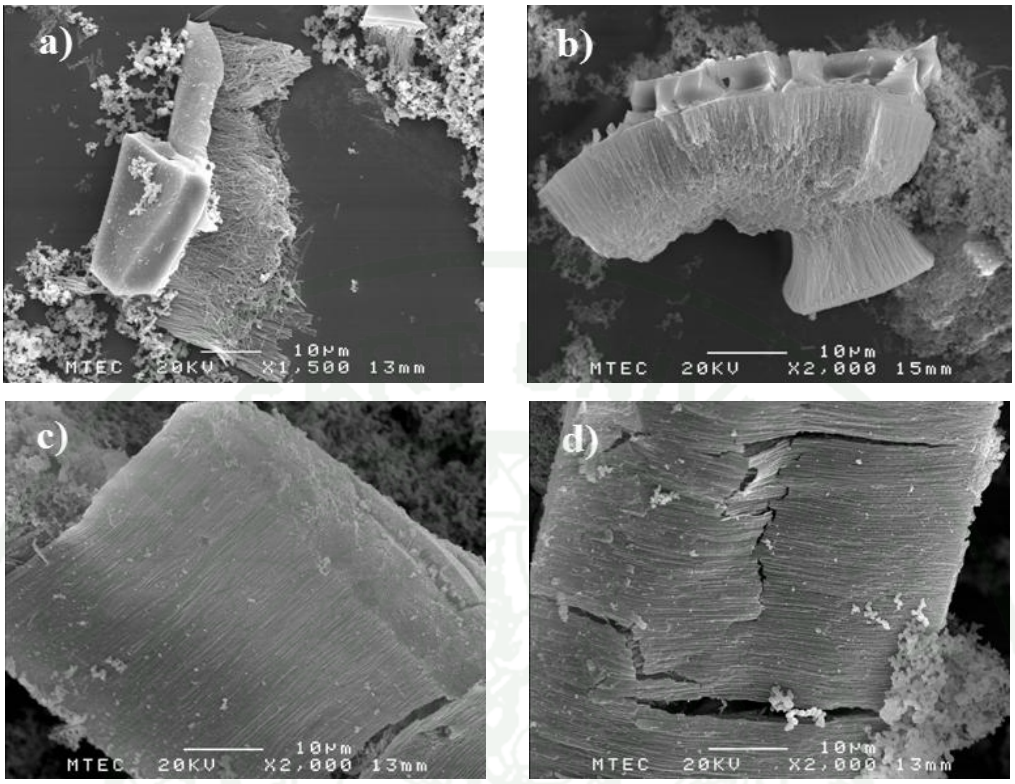

Figure 9 SEM images of perfect nanotube array prepared by template-assisted synthesis of the dispersion (a) TAPW - 4100, (b) TAPW - 1113, (c) TAPW - 11203 and (d) TAPW - 11203 (70°C).

However, the amount of perfect nanotube array was incomparable to the whole product observed. The majority proportion of samples appeared as a cracked or damaged tube in all preparation (Figure 10). The increasing of solid content in the Ti-sol did not yield the higher quality of products even in the using of the dispersion containing the highest solid content, TAPW - 4100. Cracking behavior could be described by either the non-uniform capillary action and shrinkage of nanotube during the sintering step.

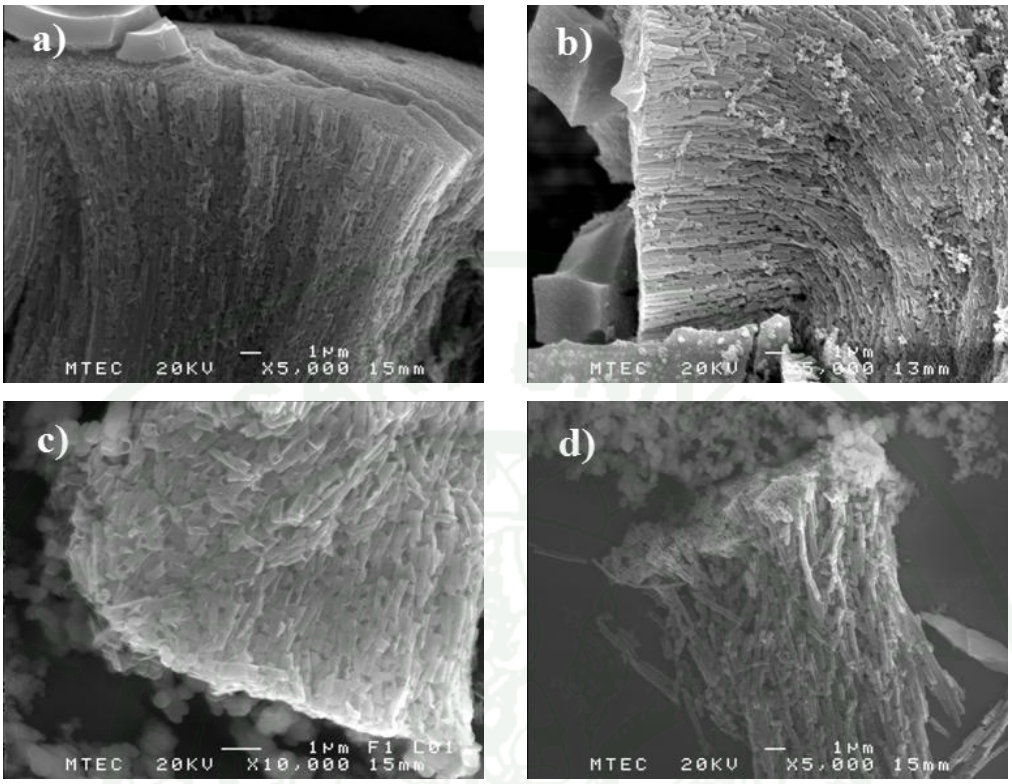

Figure 10 SEM images of the imperfect nanotube array appeared in the template-assisted synthesis from the dispersion (a) TAPW - 4100, (b) TAPW - 1113, (c) TAPW - 11203 and (d) TAPW - 11203 (70^{o}C).

Due to the difficulty to produce a large proportion of the good quality nanotube, therefore, the hydrothermal method was used instead of the template-based method to make the promising electrode.

2. Hydrothermal crystallization of TiO_2 : an effect of anion species

TiO_2 was hydrothermally crystallized in the presence of chloride (Cl^-) ion and compared with those synthesized in the presence of sulfate (SO_4^{2-}) ion. Typically, the products obtained from both cases appeared as white film deposited on the teflon-liner surface. SEM investigation showed that the TiO_2 film crystallized in the presence of Cl^- ions was consisted of the dandelion-like microflower (Figure 11). An average diameter was 12 ± 1 μm. Each microflower was consisted of a number of rectangular nanorods, randomly radiated from the central region. On the contrary, different crystal morphology of the product was observed in the case of using SO_4^{2-} solution (Figure 12). SEM analysis showed that, the film comprised the nanosized spherical crystals with an average size of 0.14 ± 0.02 μm.

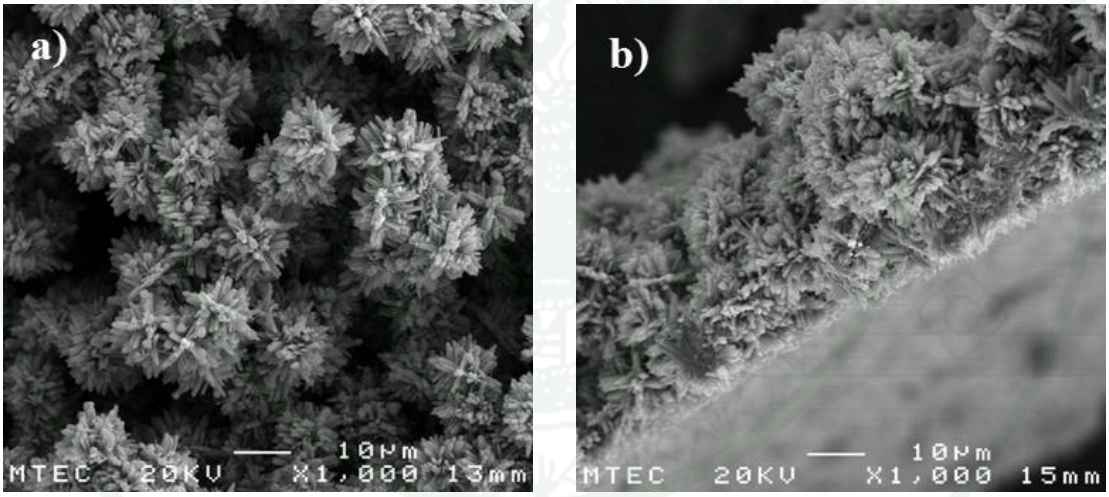

Figure 11 SEM micrographs of TiO_2 film synthesized in the presence of Cl^- ion. The product was collected from teflon-liner surface (a) top-view and (b) side view images.

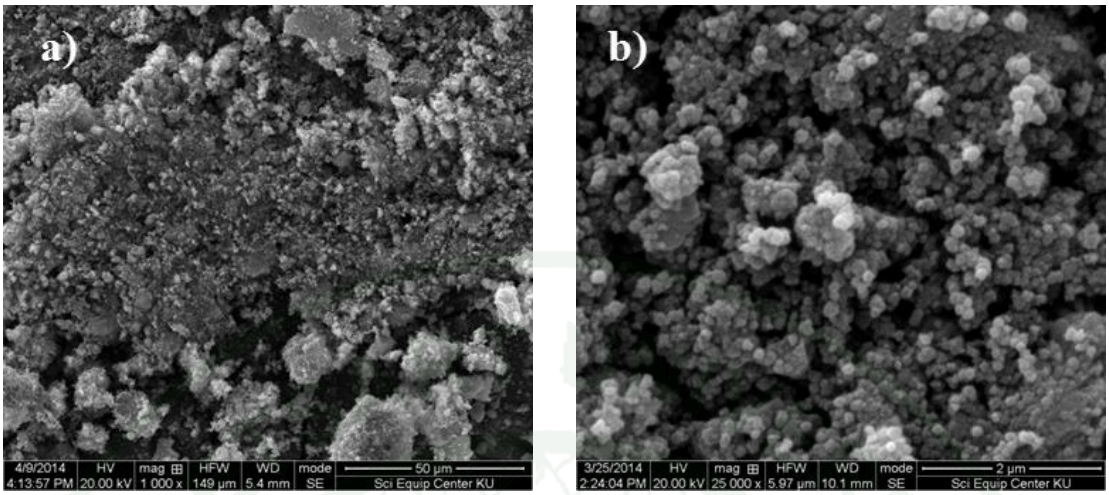

Figure 12 SEM micrographs of TiO_2 film synthesized in the presence of SO_4^{2-} ion. The product was collected from teflon-liner surface, (a) top-view image and (b) image at high magnification.

XRD technique was used to analyze the crystal structure of the products. XRD analysis of the microflower synthesized in the presence of Cl^- ions showed the reflection consistent with those of the rutile phase of TiO_2 (Figure 13a, PDF : 00-021-1276). On the contrary, the diffractogram of the spherical crystals synthesized in the presence of SO_4^{2-} ions (Figure 13b) matched to the anatase phase (PDF : 03-065-6714). The results indicated the selective role of anion on the promotion of different crystallization of TiO_2.

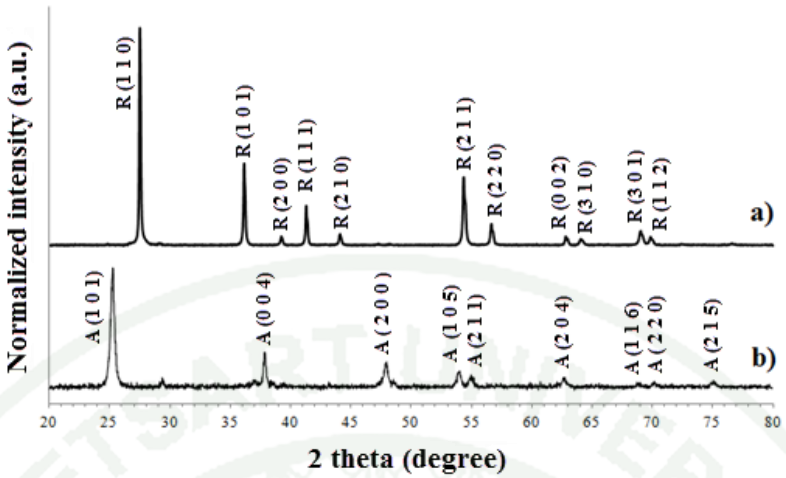

Figure 13 X-ray diffractograms of the TiO_2 films synthesized in the presence of (a) Cl^- and (b) SO_4^{2-} ions (R = Rutile and A = Anatase phase. The Miller's indices were given in a bracket.

The obtained results were consistent with previous reports (Mali *et al.*, 2013 and Ye *et al.*, 2013). The rutile phase was preferably formed in the presence of Cl^- ion, whereas the SO_4^{2-} ion promoted the formation of the anatase phase (Li *et al.*, 2011 and Yan *et al.*, 2005). The role of anions was generally described by a simple model of the trimer configuration, constructed from the octahedral [TiO_6] units (Figure 14). Initially, two [TiO_6] units shared their edges during the condensation process and, as a result, produced a dimer. Then, the third [TiO_6] unit joined the dimer to elongate the polymer chain. Importantly, the phase of TiO_2 was determined according to the sharing configuration of the third coming one (Li *et al.*, 2011 and Yan *et al.*, 2005). If the trimer was produced in a linear chain configuration, the rutile phase was resulted. In contrast, if the trimer was obtained in the zigzag chain configuration, it was determined as the anatase.

The SO_4^{2-} ion has been recognized as the anatase promoter. It was believed to act as a bidentate ligand in the octahedral coordination complex of Ti(IV). The formula of the complex was suggested as $[Ti(OH)_2(H_2O)_2SO_4]^0$ (Li *et al.*, 2011). According to proposed mechanism, the dimerization of the octahedral monomer led to the presence of sulfate at the terminal. The elongation of the octahedral chain in the

terminal direction was prohibited by steric hindrance from the anion. Therefore, the zigzag configuration was initiated, leading to the anatase structure (Figure 14).

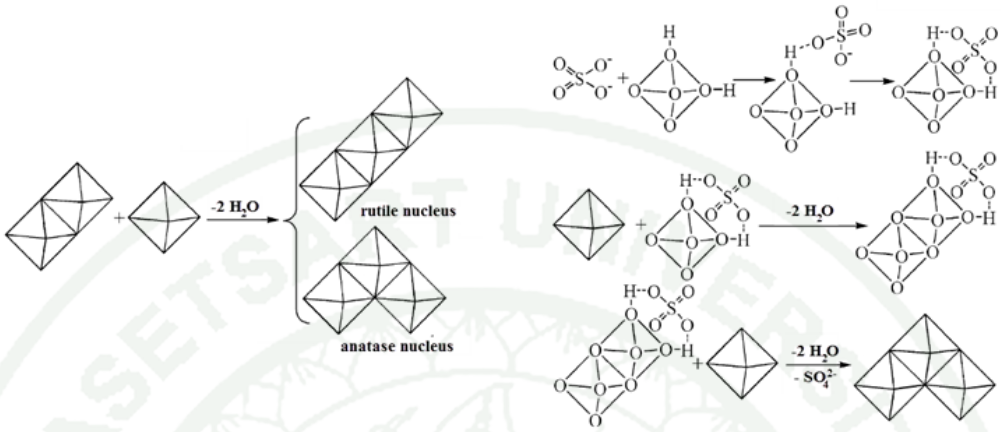

Figure 14 Proposed mechanism demonstrated the formation of anatase nuclei in the presence of SO_4^{2-} ion.

Source: Yan *et al.* (2005)

In contrast, Cl^- anion is a monodentate ligand which has lower complexing affinity than the SO_4^{2-}. The Cl^- was found in various forms in the octahedral Ti(IV) complex, such as $[Ti(OH)_2Cl(H_2O)_3]^+$ and $[Ti(OH)_2Cl_2(OH_2)_2]$, depending on the concentration of Cl^- in the solution (Pottier *et al.*, 2001).

The starting complex used to build the linear octahedral chain was unclearly identified. At first, $[Ti(OH)_2Cl_2(H_2O)_2]^0$ seemed to be the starter unit of brookite, whereas the lower number of Cl^- in the octahedral Ti(IV) complex, which led to the higher number of OH^- ligand, seemed to be the favorable starter unit for rutile (Pottier *et al.*, 2001 and Zhang and Gao, 2003). However, it was supposed that the trans-configuration of $[Ti(OH)_2Cl_2(H_2O)_2]^0$ should be an appropriate form (Li *et al.*, 2011).

The less affinity of Cl^- made it the better leaving group in comparison with SO_4^{2-}. Therefore, polymerization of octahedral complex could be carried out in the linear direction via the releasing of both H_2O and HCl, resulting in the rutile structure.

The results confirmed the selective role of Cl^- and SO_4^{2-} ions in the promotion of the rutile and the anatase phase, respectively. Moreover, this method was beneficial in producing highly pure phase of TiO_2 without any further heat-treatment.

3. Hydrothermal synthesis of the 1-D nanostructured TiO_2 on the FTO substrates

The objective of this study is to form 1-D nanostructured TiO_2 on a transparent conductive material. Although the array of TiO_2 nanotubes could be produced by the template-based method, the quality of the products was poor, due to the large degree of cracking. Alternatively, hydrothermal method was used to synthesize the 1-D nanostructured TiO_2 instead of the template-based method.

It was known from the previous section that the hydrothermal synthesis gave either microflower like or nanosized spherical crystal, depending on the anion used. In both cases, crystallization took place on the surface of the teflon liner. The same hydrothermal condition was used in this study. The FTO glass substrate was placed in the reaction mixture to induce the formation of TiO_2 on its surface.

SEM analysis of the white solid on the FTO substrate, obtained from the synthesis in the presence of Cl^- ions, showed a number of microflower-like crystals (Figure 15a). The microflower-like crystal was consisted of rectangular-shaped nanorods, which were similar to those obtained without the FTO substrate. Further investigation revealed an additional layer between the microflower and the substrate surface (Figure 15b). This layer was composed of vertically aligned rectangular nanorods.

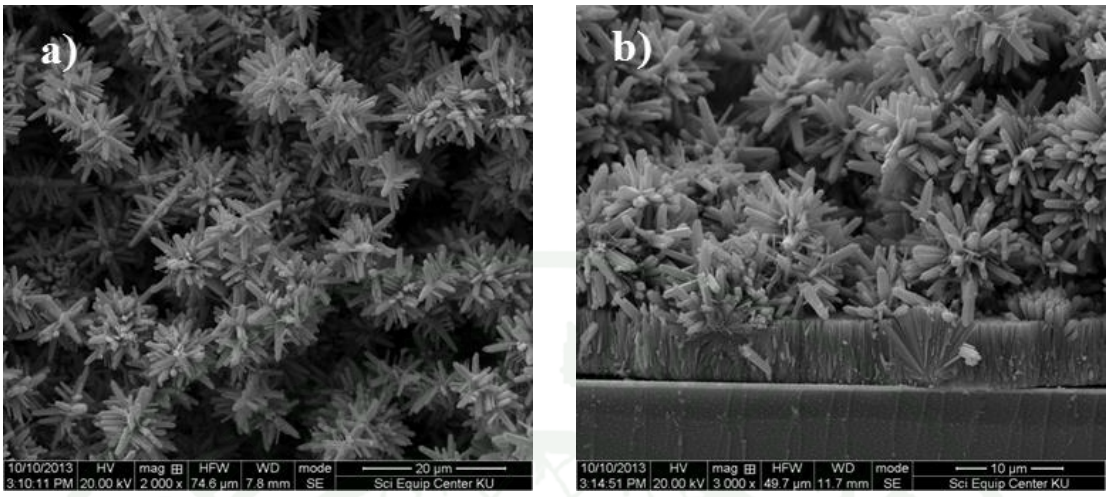

Figure 15 SEM images of TiO_2 film synthesized in the presence of Cl^- ion on FTO substrate, (a) a top view and (b) a side view.

The uniform array of the nanorods suggested that the nanorods layer grew from the FTO surface whereas the microflower appeared to form directly in the solution phase. The microflower become larger and gradually fell on top of vertically aligned nanorod layer. A separate synthesis was carried out by holding the FTO substrate vertically with respect to the bottom of the teflon liner in order to confirm the formation of uniform nanorods. SEM analysis showed that only the uniform nanorod array was observed on the FTO substrate (Figure 16), confirming that the formation of the nanorods started at the FTO surface. The high magnification image revealed that each nanorod comprised a bunch of nanoneedles (Figure 16b) (Ye *et al.*, 2013).

In the case of using SO_4^{2-} ions, SEM analysis demonstrated that the synthesized TiO_2 film was consisted of spherical shaped crystals deposited on the FTO surface (Figure 17). The average particle size was 2.7 ± 0.2 µm. Note that, the presence of 1-D nanostructure was not observed. Only the thin layer with certain thickness was found under the layer of spherical crystals.

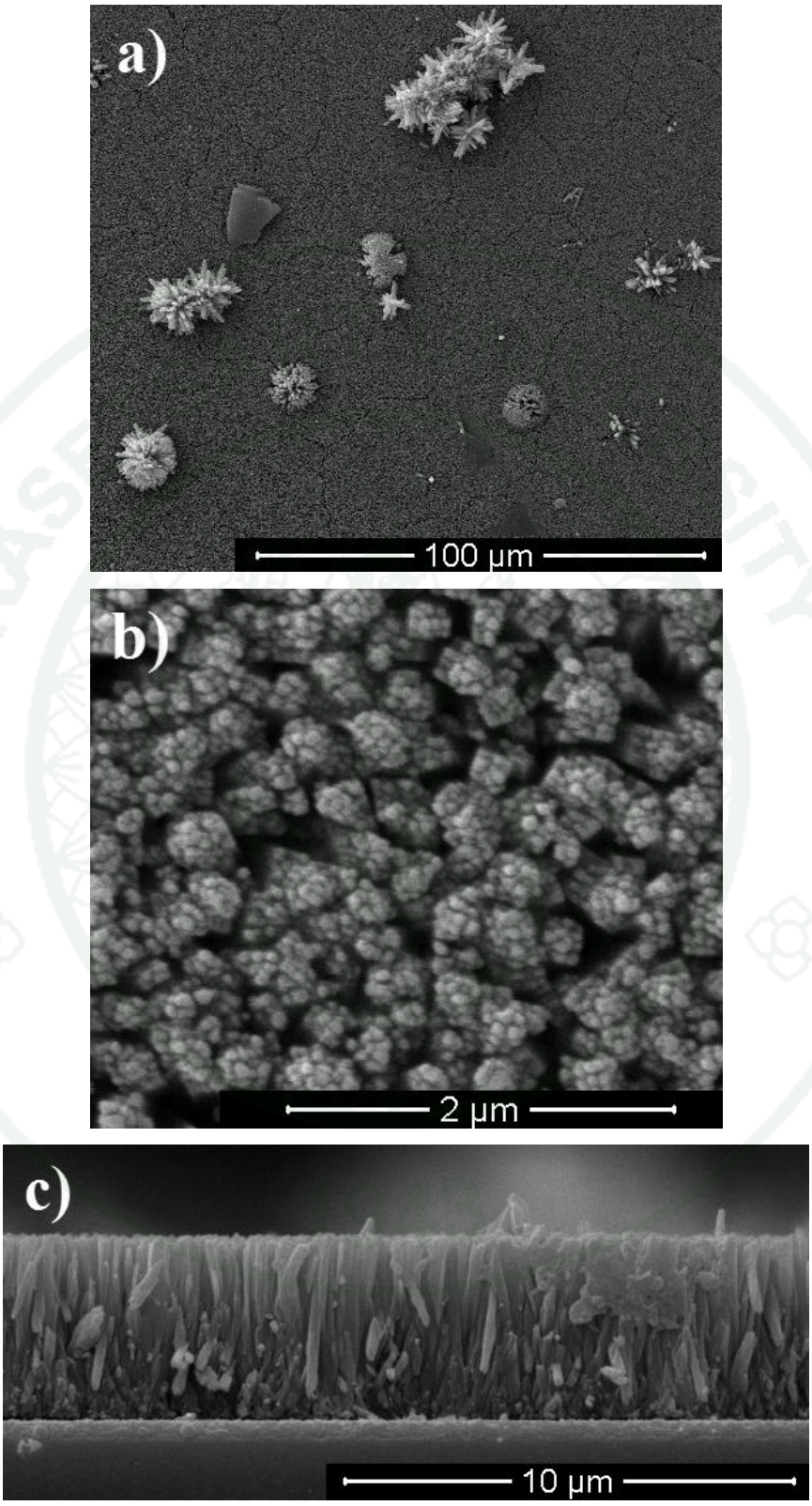

Figure 16 SEM images of TiO_2 film synthesized in the presence of Cl^- ion on FTO substrate, (a-b) a top view and (c) a side view.

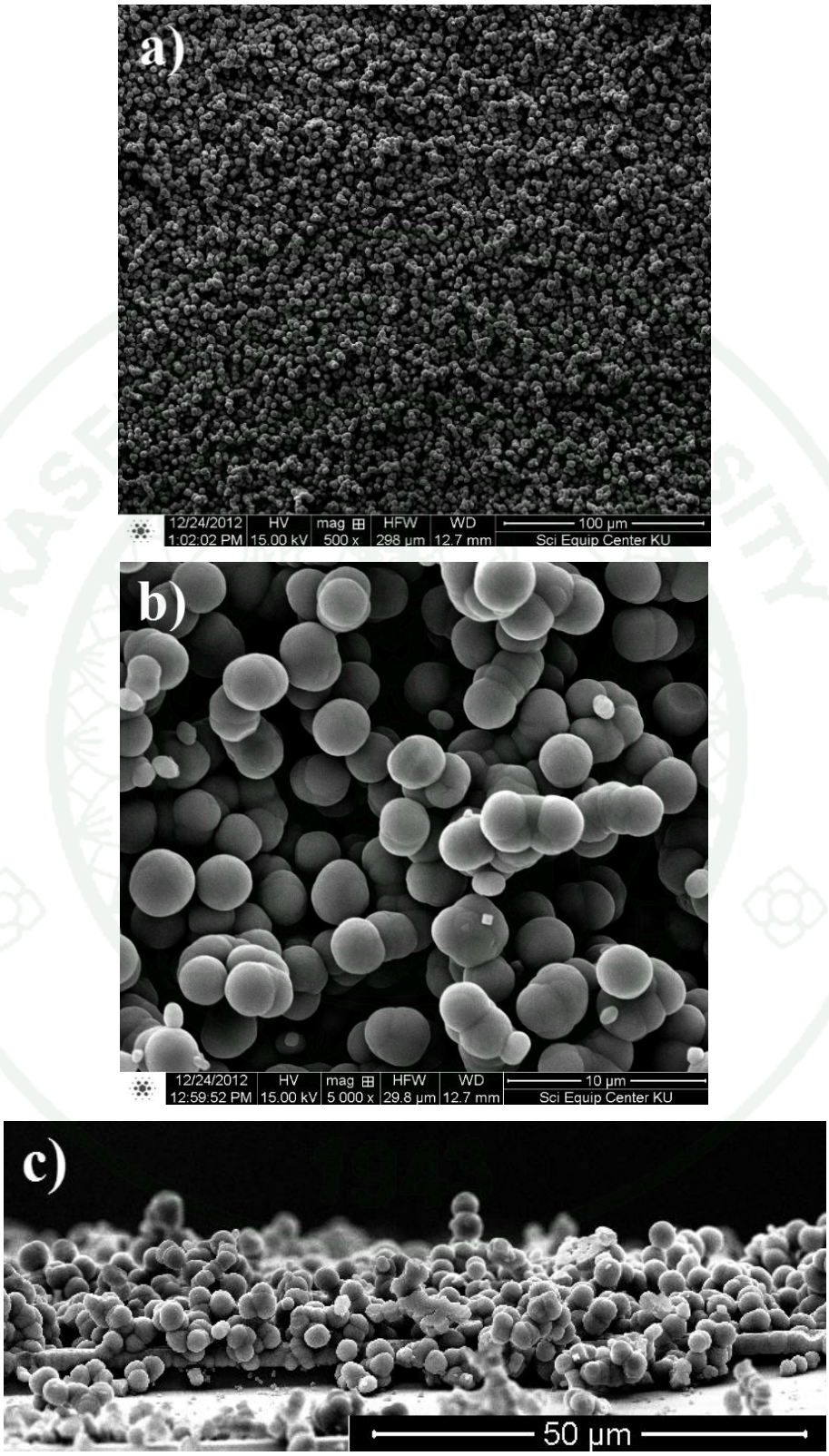

Figure 17 SEM images of TiO_2 film synthesized in the presence of SO_4^{2-} ion on FTO substrate; (a-b) a top view and (c) a side view.

Similar to the case of using Cl^- ion, holding the FTO substrate vertically during the synthesis removed those large spherical crystals, therefore, only the thin layer of equal thickness was clearly observed on the FTO surface (Figure 18).

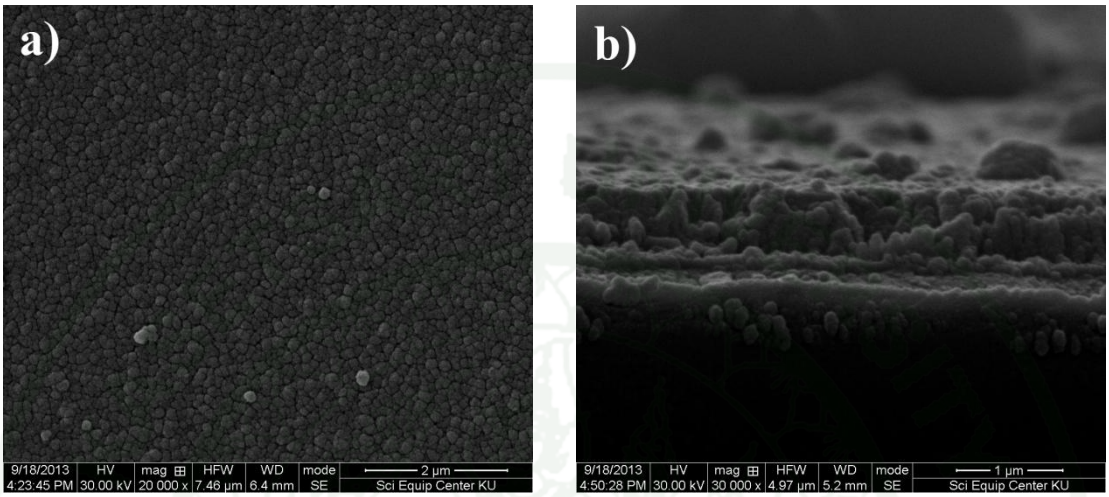

Figure 18 SEM images of the TiO_2 film synthesized in the presence of SO_4^{2-} ion on FTO substrate; (a) a top view and (b) a side view.

XRD analysis of the product synthesized in the presence of Cl^- ion showed the reflection consistent with the rutile TiO_2 (Figure 19a, PDF : 00-021-1276). On the contrary, investigation of the product synthesized in the presence of SO_4^{2-} showed the reflection consistent with the anatase TiO_2 (Figure 19b, PDF : 03-065-6714). In both cases, the reflections corresponding to the rutile SnO_2 was also observed (Figure 19c, PDF : 01-070-6995). This was attributed to the rutile SnO_2 layer of the FTO substrate.

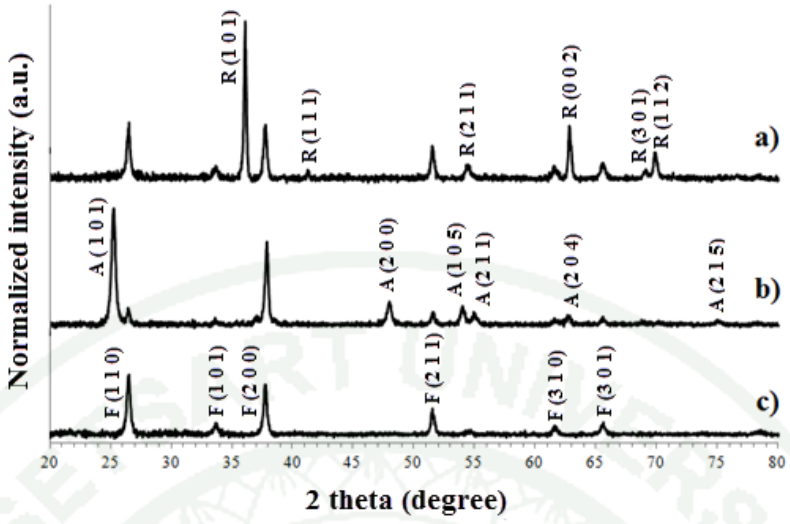

Figure 19 X-ray diffractograms of the TiO_2 film on the vertically placed FTO substrate, synthesized in the presence of (a) Cl^- ions and (b) SO_4^{2-} ions. (c) Diffractogram of bare FTO substrate, showing the reflection of the rutile SnO_2.

4. Growth of the preferred oriented rutile TiO_2 nanorods on the FTO substrate

In previous section, the results demonstrated that only the 1-D nanostructured rutile TiO_2 was formed on the FTO substrate. The vertical alignment of the rutile phase specifically occurred on the SnO_2. In the case of anatase phase, the 1-D nanostructure was not formed. Hence, the growth of the 1-D nanostructured rutile TiO_2 on the FTO substrate was believed to associate with the SnO_2 layer of the substrate.

Control synthesis in a presence of Cl^- ion using a normal glass slide instead of the FTO substrate was carried out in order to confirm the role of the SnO_2 layer. SEM analysis of the TiO_2 film produced on either horizontally or vertically placed the glass slide did not show any appearance of the vertically aligned nanorod (Figure 20 and 21). Typically, the products on the glass substrate seemed to be similar as those obtained on the teflon liner (see also Figure 11). Therefore, the result confirmed the crucial role of the SnO_2 layer in the growth of the 1-D nanostructured TiO_2 on the FTO substrate.

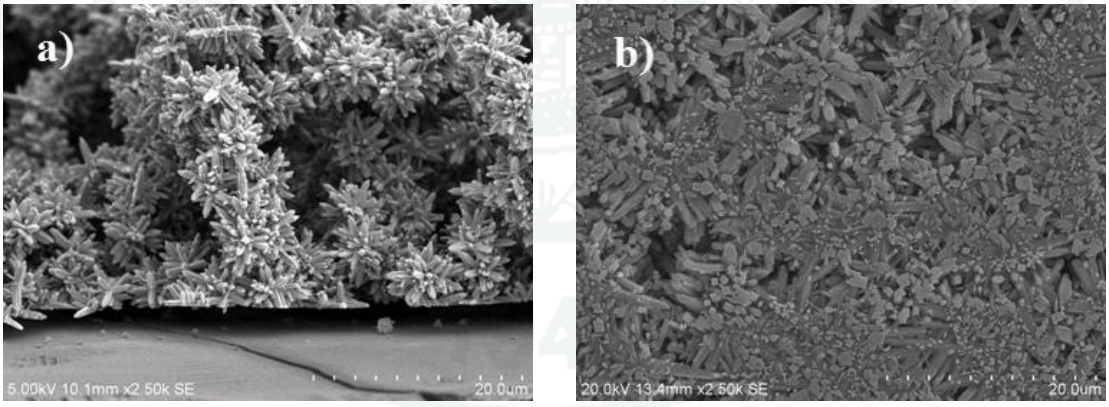

Figure 20 SEM images of TiO_2 film synthesized in the presence of Cl^- ion on horizontally placed glass substrate; (a) a side view and (b) a bottom view of the TiO_2 film.

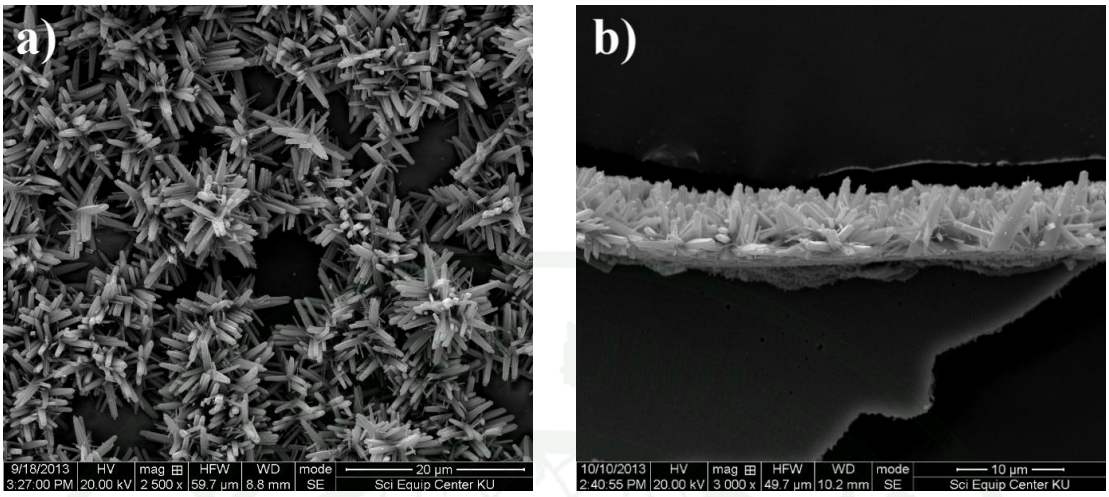

Figure 21 SEM images of TiO_2 film synthesized in the presence of Cl^- ion on the vertically placed glass substrate; (a) a top view and (b) a side view of the TiO_2 film.

XRD analysis of the synthesized TiO_2 on the glass substrate showed that the product was the rutile TiO_2 (Figure 22, PDF : 00-021-1276) which similar to the results of those obtained on teflon liner surface (Figure 13a). However, the diffraction pattern of rutile microflower on glass and teflon substrates were different form the vertically aligned rutile nanorods on FTO substrate (Figure 19a).

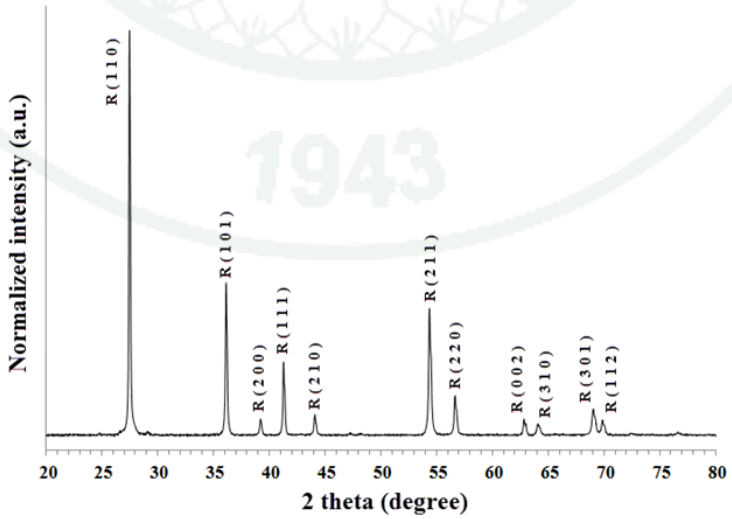

Figure 22 XRD diffractogram of the synthesized TiO_2 on glass substrate.

In Figure 19a, the reflection of (110), (220) planes, which was observed as the sharp peaks in the common diffractogram of rutile TiO_2, was disappeared. Moreover, the intensity of (111) and (211) planes significantly decreased, while, reflection of (002) plane was dominant in the diffractogram. The behavior could be described by preferred orientation and would be discussed later (Gratta-Bellew, 1975, Yang et al., 2011).

TEM and SAED were performed to understand the arrangement of crystal planes in nanorod. It is generally known that tetragonal rutile structure possesses four types of low index crystal plane, (110), (100), (101) and (001) (Diebold, 2003). SAED analysis showed sharp diffraction spots suggesting that the nanorod was single-crystalline (Figure 23b). Interpretation of diffraction pattern indicated that the nanorod was elongated along the [001] direction whereas the (110) plane was exposed as nanorod side wall (see also Appendix B) (Hosono et al., 2004 and Zhu et al., 2011). The result was consistent with the previous report demonstrated that the (001) was the most active facet of rutile TiO_2, due to its relatively high surface energy. The relative surface energy could be sorted as (110) < (100) < (101) < (001) (Perron *et al.*, 2007).

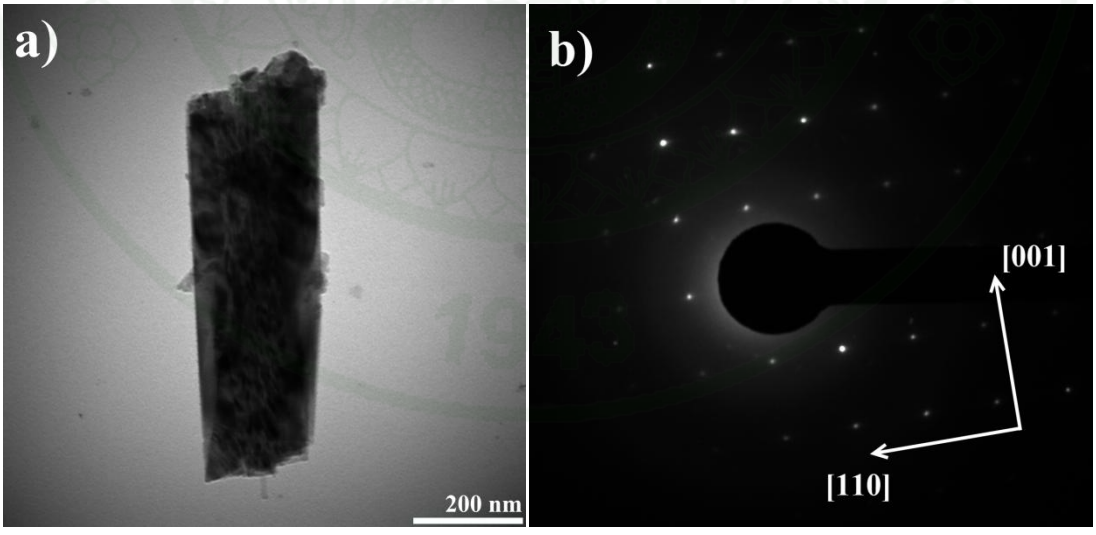

Figure 23 (a) TEM image and (b) selected-area electron diffraction (SEAD) pattern of the rutile TiO_2 nanorod on the FTO substrate.

The rutile TiO_2 was believed to pseudomorphically grow on the rutile SnO_2 surface by epitaxy relationship (Liu and Aydil, 2009 and Park et al., 2012). A small lattice mismatch, typically less than 15%, of the atomic arrangement between two minerals permitted the heteroepitaxy (Herman, 2004). In the case of rutile TiO_2 and rutile SnO_2, the promotion factors were not only the similarity of crystal structure, but also their unit cell parameters were very similar (Batzill and Diebold, 2005). The calculated mismatches of unit cell parameters among a-axis and c-axis were 3.16% and 7.21%, respectively (Appendix C), that presumably allowed the creation of epilayer on the SnO_2 substrate.

Heteroepitaxy of rutile TiO_2 on rutile SnO_2 was explained in many study by concerning the important condition that the exposed plane of single-crystalline substrate has to be known before the synthesis (Budak et al., 2006, Zhuge et al., 2012 and Rosental et al., 2013). In this work, the explaining of the heteroepitaxy between rutile TiO_2 and rutile SnO_2 was complicated because of the sputtered SnO_2 layer of FTO substrate was the polycrystalline film. Hence, it was unable to specify the exposed facet of SnO_2 on the substrate. The another possible ways to explain the formation rutile nuclei on FTO surface would be the cause of surface roughness of substrate and followed by the growth of nanorod via vapor-solid (VS) growth (Martin et al., 2010, Wang et al., 2010 and Zhuge et al., 2012). The sputtered SnO_2 layer exhibited the rough surface which also promoted the deposition of adatom or growth unit, resulting in the active site on SnO_2 surface (Martin et al., 2010 and Yang et al., 2011).

After the nucleation step, the rutile TiO_2 nuclei preferentially grew along the [001] direction with the fastest growth rate, whereas, the growth along [110] direction was proceeded with the slowest growth rate due to the relative surface energy of rutile as confirmed by TEM and SAED (Zhuge et al., 2012). In addition, the (110) face was reported to preferentially absorb by Cl^- ion, and then the expansion of crystal along [110] direction was retarded (Li *et al.*, 2009). Moreover, flux of $[TiO_6]$ growth unit must supplied from a direction above the film, led to the preferential growth of rutile nanorods out of the plane of substrate surface.

1-D nanostructured film of the (001) preferential growth rutile TiO_2 nanorods resulted in the preferred orientation film which could be observed the behavior by XRD (Gratta-Bellew, 1975, Yang et al., 2011). The diffraction of the preferred oriented nanorod film showed the lack of (110) and (100) reflections (Figure 19a). Moreover, the relative (002)/(101) peak area ratio of the oriented nanorod film was higher than those calculated from random oriented nanorods (Figure 22) about 4 times (Yang et al., 2011). To confirm the conclusion, random oriented nanorods sample, prepared from the sample of Figure 19a by scratching and grinding, was used to analyze. The random oriented nanorods showed the diffractogram similar to the diffraction of typical rutile TiO_2 samples (Figure 13a and Figure 22), that implied an absence of preferred oriented behavior (Figure 24).

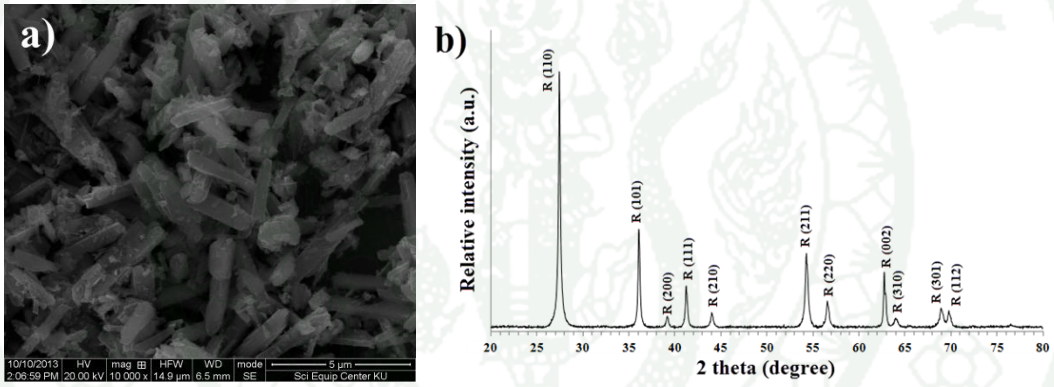

Figure 24 The random oriented rutile TiO_2 nanorods scratched from the 1-D nanostructured TiO_2 film on FTO substrate and followed by grinding. (a) SEM image of the sample and (b) XRD diffractogram of the sample spread on Si wafer.

Temperature-dependent synthesis of the 1-D nanostructured TiO_2 on the FTO substrate was carried out using 20 ml of T_0.4 solution. Decreasing of synthesis temperature dramatically affected nanorod length (or the thickness of the TiO_2 nanord film) owing to the slower growth rate (Figure 25). The number of nanorod per unit area increased when the temperature was decreased from 180 ^oC to 120 ^oC. However, this factor resulted in the opposite trend on the changing of nanorod diameter. Histogram showing the distribution of nanorod diameter indicated the decreasing of

population of the large diameter when the synthesis temperature was decreased (Figure 26). The nanorod synthesized at low temperature (140 ^{o}C) seemed to be more uniform in diameter than those synthesized at high temperature (180 ^{o}C). However, the TiO_2 nanorods on the FTO substrate was not obtained from the synthesis at 120 ^{o}C.

Equally important, concentration-dependent experiment was also studied with using of T_0.2, T_0.4, T_0.6 and T_0.8 solutions. By carrying the same hydrothermal condition, lowering the amount of TTIP resulted in the decreasing of film thickness (Figure 27). It was noted no TiO_2 nanorods were observed in the case of using T_0.2 solution. It could be ascribed to the concentration of $[TiO_6]^{2-}$ complex in the solution which did not reach the supersaturation limit. Hence, the dissolution process overwhelmed the crystallization process leading to the absence of product on the FTO substrate.

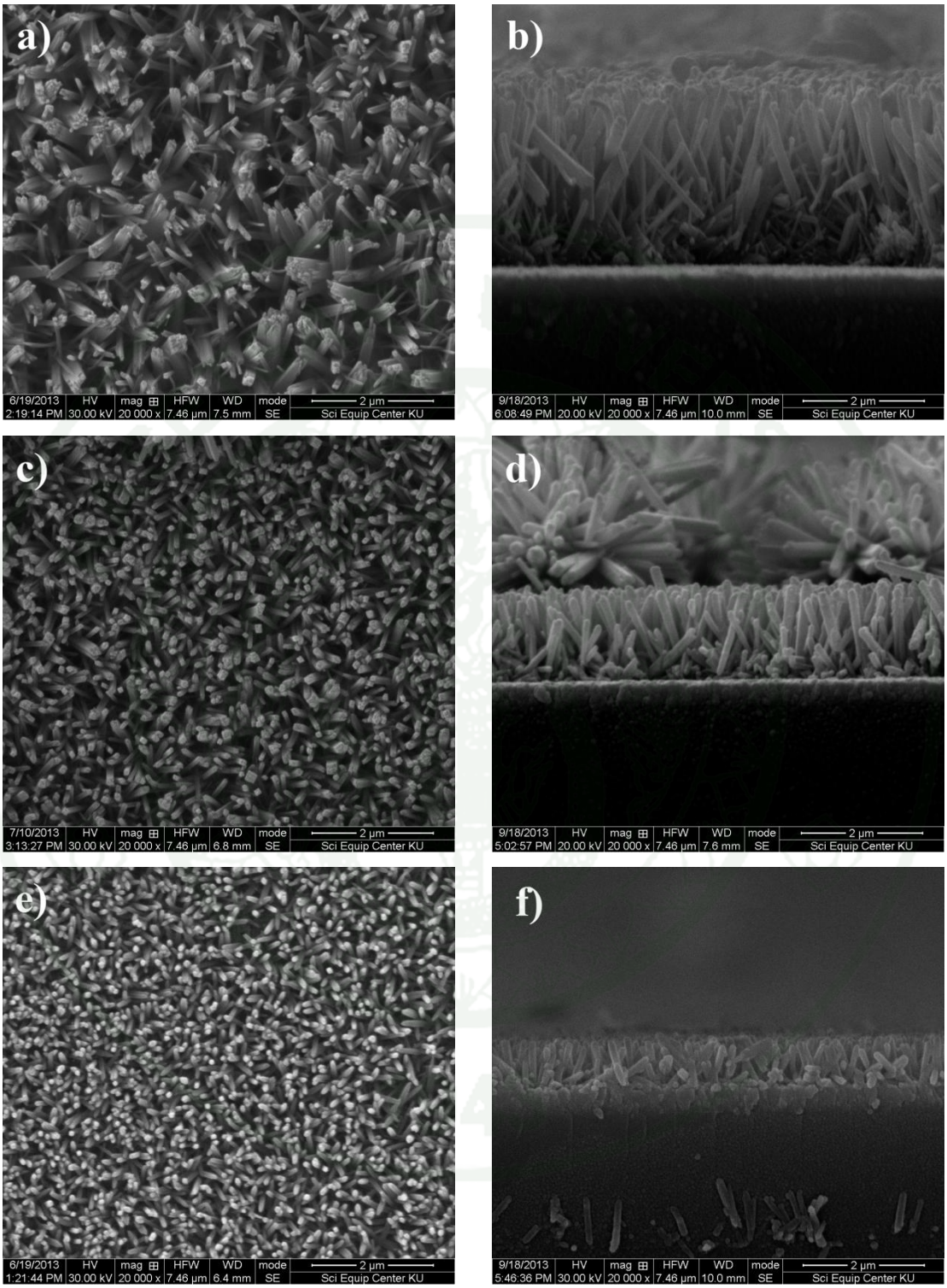

Figure 25 SEM images of the TiO_2 films synthesized by using T_0.4 solution at different temperatures, (a-b) 180 ^{o}C, (c-d) 160 ^{o}C and (e-f) 140 ^{o}C.

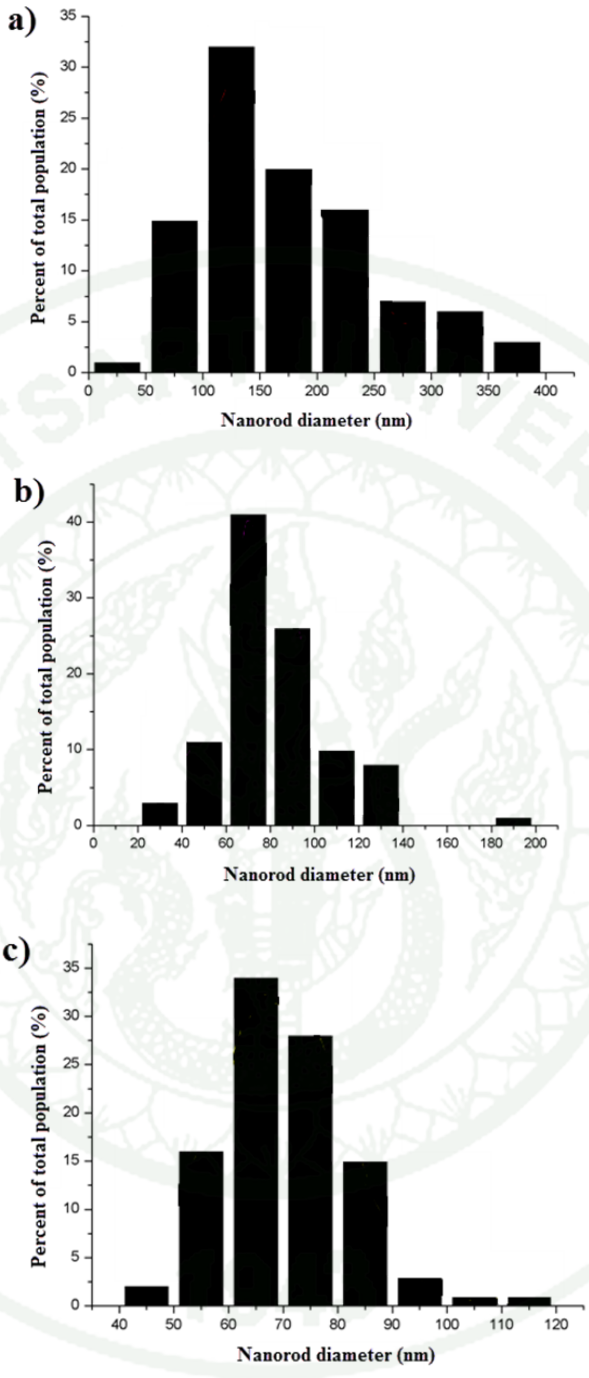

Figure 26 Histogram of nanorod diameter of the 1-D nanotructured TiO_2 on FTO substrate, synthesized from T_04 solution at (a) 180 ^{o}C, (b) 160 ^{o}C and c) 140 ^{o}C, respectively.

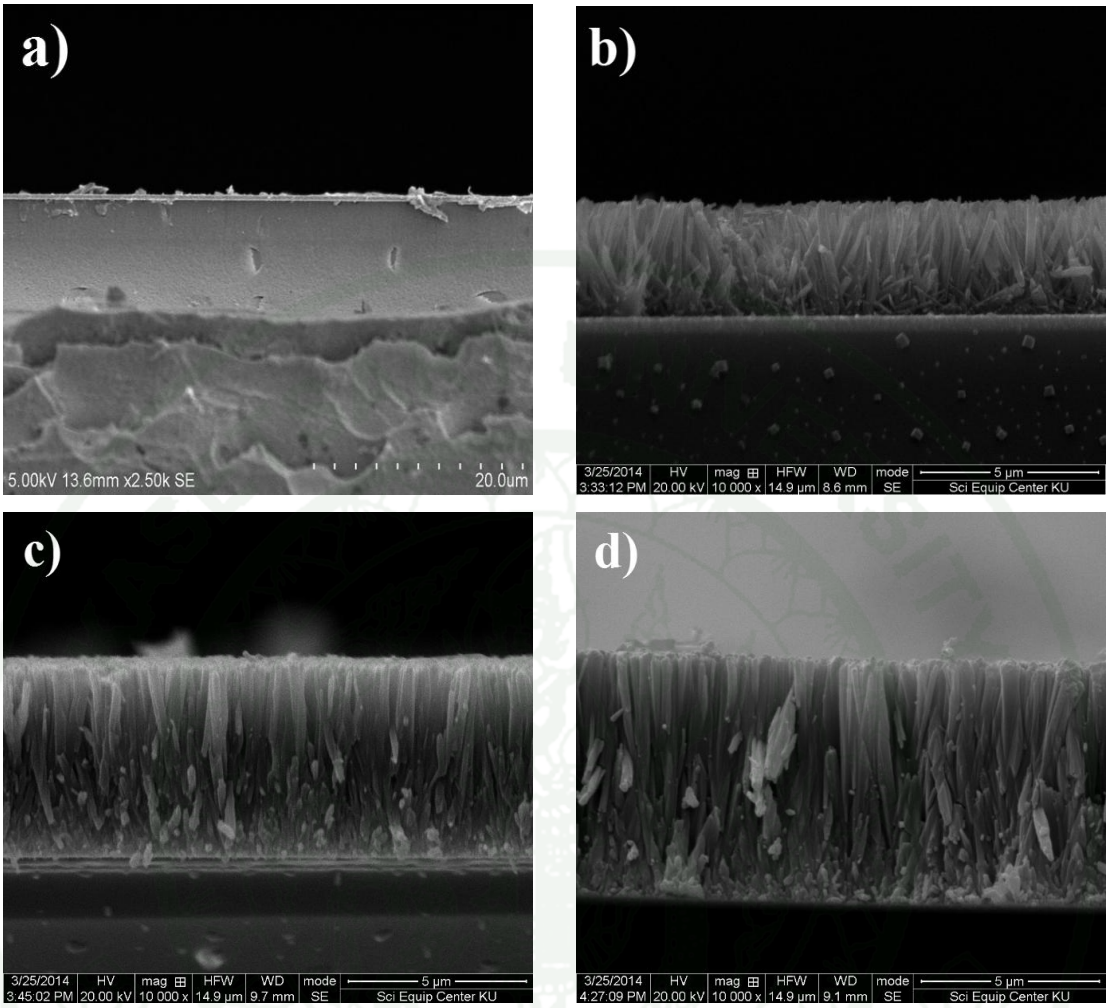

Figure 27 SEM analysis of the TiO_2 films synthesized at 180 ^oC using (a) T_0.2, (b) T_0.4, (c) T_0.6 and (d) T_0.8 solutions.

The synthesized 1-D nanostructured TiO_2 electrodes of the concentration-dependence experiment in Figure 27(b-d) were named as NR-T_0.4, NR-T_0.6 and NR-T_0.8, according to the precursor solution used. They were employed as a working electrode in the EIS study and compared with the nanoparticle-based electrodes, P25 and P25_900. SEM investigation of nanoparticle electrodes, P25 and P25_900, showed the densely packed film of TiO_2 nanocrystals on FTO substrate (Figure 28). Thickness of TiO_2 layer of all electrodes in EIS study were measured and reported in Table 3.

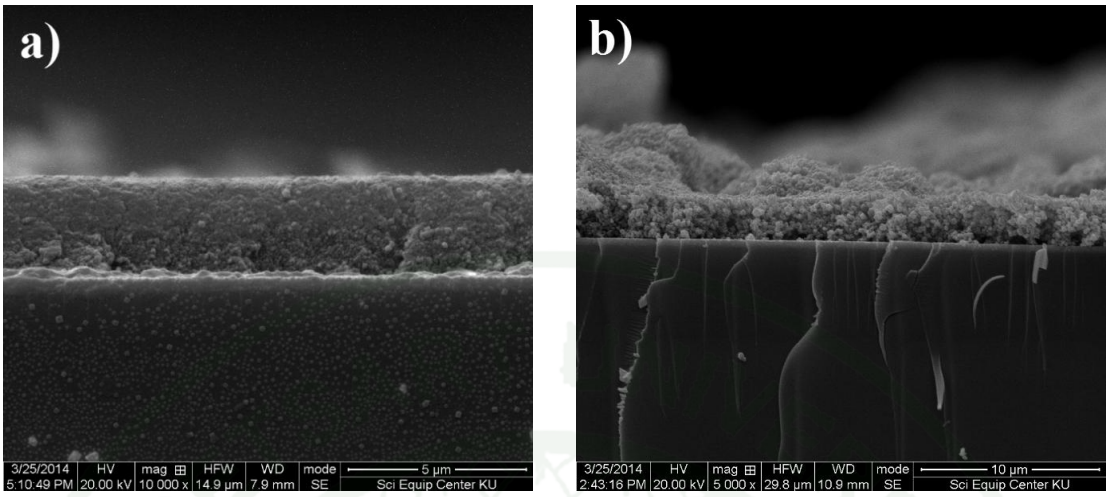

Figure 28 SEM images of the colloidal TiO_2 electrodes, (a) P25 and (b) P25_900.

Table 3 Average film thickness of the as prepared TiO_2 electrodes in the EIS experiment

Electrode name	Average film's thickness (µm)
NR-T_0.4	3.2 ± 0.1
NR-T_0.6	5.4 ± 0.1
NR-T_0.8	6.8 ± 0.5
P25	3.2 ± 0.4
P25_900	2.4 ± 0.7

Crystal structure of the TiO_2 nanoparticles electrode was analyzed by XRD. The first control, P25, showed the reflection (Figure 29a) of the anatase TiO_2 (PDF : 03-065-6714),, while the reflection of the second control, P25_900 (Figure 29b), consistence to the reflection of rutile phase (PDF : 00-021-1276). Additional reflection in the diffractograms could be referred to the rutile SnO_2 of FTO substrate.

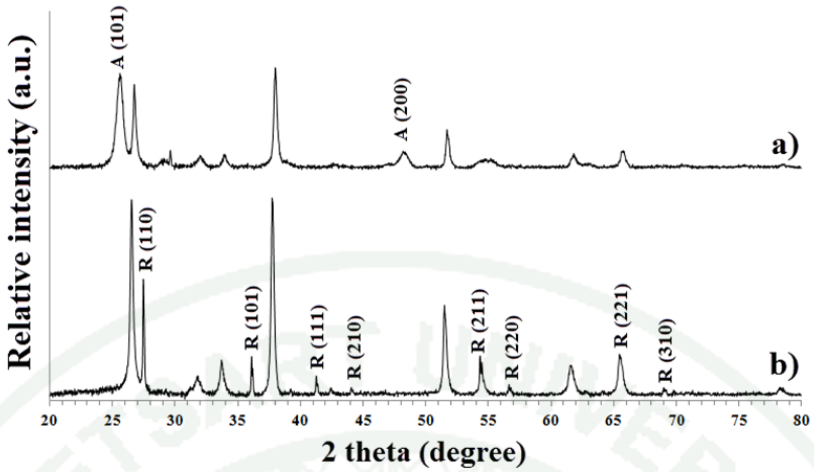

Figure 29 X-ray diffractograms of the colloidal TiO_2 electrodes (a) P25 and (b) P25_900.

5. Electrical performance of the synthesized TiO_2 electrode by electrochemical impedance spectroscopy (EIS)

Electrical resistance (R) is an important parameter to determine performance of the synthesized electrode. This parameter is generally investigated by electrochemical impedance spectroscopy (EIS). In this study, the electrical resistance of the synthesized 1-D nanostructured TiO_2 electrodes, NR-T_0.4, NR-T_0.6 and NR-T_0.8 were compared with the results from nanoparticle-based electrodes, P25 and P25_900 (see Table 2 and 3).

Electrochemical impedance spectroscopy (EIS) is an analytical technique to investigate the dielectric properties of samples (Lvovich, 2012). This technique measures the sample impedance (Z) over a wide range of applied frequencies in AC circuit. It is based on the general concept of Ohm's law which define as

$$Z = \frac{V}{I}$$

where Z is the electrical impedance in a unit of ohm (Ω)
V is the applied voltage in a unit of Volt (V)
and I is the electrical current in a unit of Ampere (A)

Electrical impedance (Z) is referred to the total resistance generated from the common electrical circuit elements such as resistor (R), capacitor (C) and inductor (L), and also defined as the total impedance

$$Z = R + iX$$

where R is the real part of electrical impedance (resistive impedance).
and X is the imaginary part of electrical impedance (reactive impedance).

The imaginary part of impedance (X) is referred to the impedance from capacitor, $X_C = \omega C^{-1}$ and inductor, $X_L = \omega L$, where $\omega = 2\pi f$, and also defined as $X = X_L - X_C$ whereas ω is an angular frequency and f is an applied frequency. The plot of impedance data is usually represented by a Nyquist plot. The real part is plotted on the X-axis and the imaginary part is plotted on the Y-axis of a chart as shown in Figure 30. The plot of EIS data usually occur as a semicircular arc diagram. Diameter of semicircular diagram indicates the real electrical resistance of the circuit while the height of the diagram implies the imaginary component of the signal. The smaller size of the arc diagram implies the lower impedance. The number of semicircular arcs in the diagram exhibits the number of dielectric layer that current pass through.

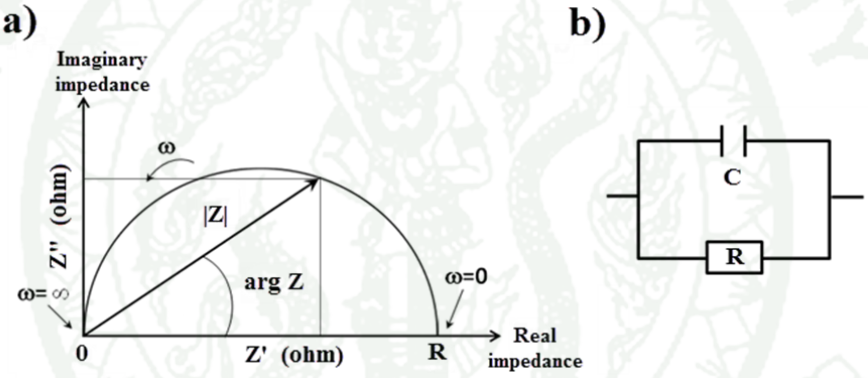

Figure 30 (a) Nyquist plot of one time constant electrical circuit (b), possessing a resistor and a capacitor.

Source: Andrade *et al.* (2011)

Figure 31 showed Nyquist plots of impedance signal from electrodes that used in the experiment. It can be seen from the figure that the responsive signal from all electrodes do not show the completed semicircular arc diagram. That implies the low responsibility of the samples owing to the electron-transfer-limited (Song *et al.*, 2008). Moreover, the small semicircular arc of electrolyte and CE at high frequency region are also unseen from the figure, due to the measurement in the dark condition (Song *et al.*, 2008).

In Figure 31a, it was clearly seen that the P25_900 electrode exhibited the largest responsive signal far from the others (Figure 31a). The result suggested that P25_900 possessed large electrical impedance than the other ones. The second high responsive signal was given by the P25 electrode (Figure 31b). According to electrode parameters, the main difference between P25 and P25_900 electrode was the crystal structure of TiO_2 that used to fabricate the electrodes, anatase structure for P25 and rutile structure for P25_900. Therefore, the results still consistence with previous study that TiO_2 in the anatase structure usually showed better electrical performance in comparison with the rutile phase (Park *et al.*, 2000).

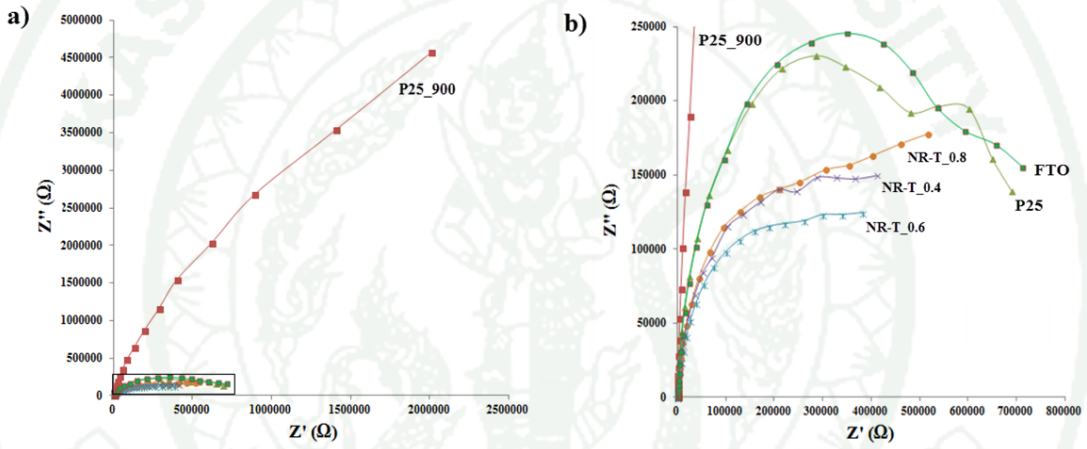

Figure 31 (a) The Nyquist plots of TiO_2 electrodes in EIS experiment and (b) the magnification of squared area in (a).

By considering the EIS signals from the 1-D nanostructure TiO_2 electrodes, it was clearly seen that all samples exhibited the lower electrical impedance than the densely packed nanocrystalline TiO_2 electrode, P25 and P25_900. Especially, by comparing the results between the 1-D nanostructure TiO_2 electrodes and the P25_900 electrode, it clearly showed the enhancement of electrical performance from the organizing the nanostructure of TiO_2 film.

However, the signal of 1-D nanostructure electrodes, for example NR-T_0.6 and NR-T_0.8, seemed to be constant at the low frequency measurement. It suggested the non-responsive behavior of the electrode at the region of applied frequency due to

the electron-transfer-limited from the measurement in dark condition (Song *et al.*, 2008). It is difficult to instantly quantify the value of real impedance from the data. Hence, the equivalent electrical circuit was generated to describe the EIS data of each electrode.

The equivalent circuit was provided to describe the electrical phenomena which occurred at the interface of electrodes. For example, Figure 32 showed the schematic illustration of electrical phenomena which occurred during the measurement. The migration of charged species in the electrolyte resulted in the first electrical resistance of the equivalent circuit, R_S. Then, the reductant species chemically absorbed on the TiO_2 surface was oxidized and the electron was transferred to TiO_2 layer. Electron were diffused through the compact TiO_2 nanocrystals film and then passed to the SnO_2 layer before drained out from working electrode at the Ohmic contact. Hence, R_{TiO2} and R_{FTO} were appeared in the equivalent circuit to imply electrical resistance from the moving charge in the TiO_2 and FTO layer. Therefore, charge transfer resistance of the synthesized TiO_2 layer could be determined by the R_{TiO2}.

However, other phenomena such as the formation of electrical double layer (Helmholtz layer) and the diffusion of charged species at the interface could occur during the transfer process. Hence, the complement function, C_1 and C_2 in Figure 32b, should be added to the equivalent circuit to realize the event on electrode interface. The complement function such as capacitance (C), constant phase element (CPE) and diffusion function of charge species were used in the work.

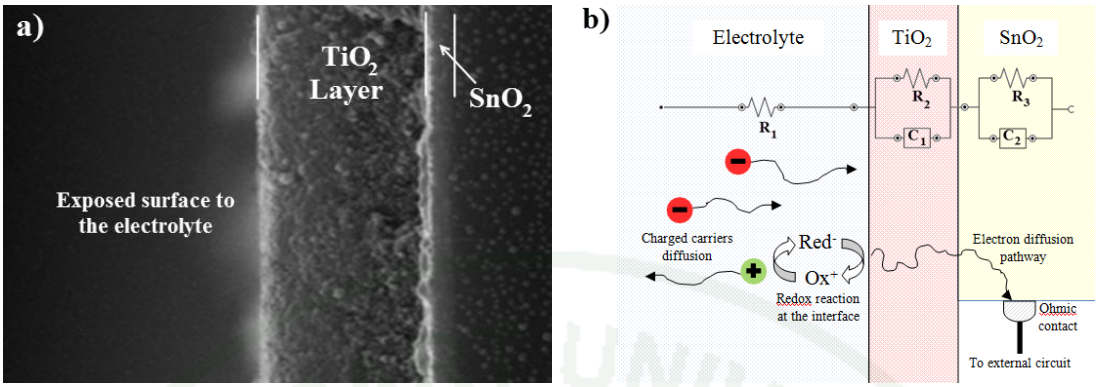

Figure 32 (a) SEM image of P25 electrode and (b) the diagram of the electrode show the main electrical phenomena on the electrode.

The equivalent circuit in this study was proposed in Figure 33. The circuit was a series connection circuit of 3 time constants, according to 2 interfaces, FTO/TiO_2 interface, TiO_2 film/ electrolyte interface (Park *et al.*, 2000, Song *et al.*, 2008 and Lvovich, 2012). R_s was introduced to the circuit due to the impedance including the resistance in electrolyte solution and the uncompensated impedance from the equipment connection. R_{TiO2} was the charge transfer resistance across TiO_2/electrolyte interface while R_{FTO} was assigned for the transfer of charge across the TiO_2/FTO interface.

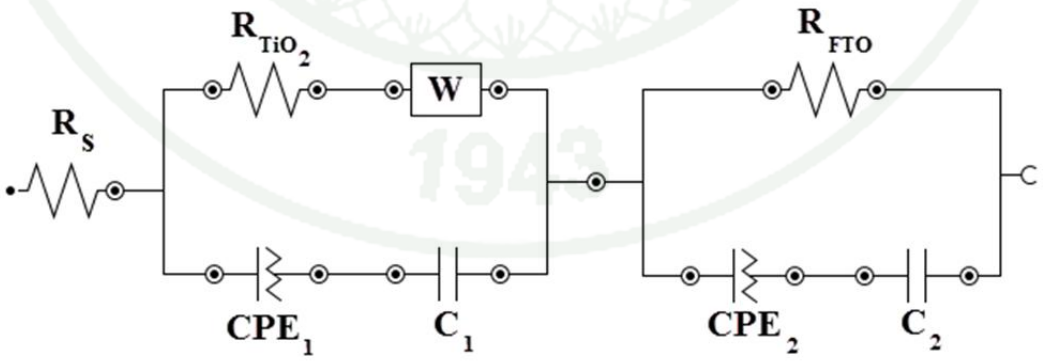

Figure 33 The proposed equivalent circuit of the as prepared TiO_2 electrodes.

R_{TiO2} and R_{FTO} were connected in parallel with the constant phase element (CPE) and capacitance (C) which referred to the surface state capacitance and the

formation of electrical double layer at the interface, respectively. Warburg impedance (W) was added to TiO_2/electrolyte interface due to the mass transfer from electrolyte to the reaction site on TiO_2 surface. Note that, to fitting the signal from P25 and P25_900, the second Warburg impedance was added to the parallel circuit of TiO_2/FTO interface to improve the fitting quality. This addition could be referred to the mass diffusion of charged specie at the electrolyte/FTO interface, due to the existing porous in the nanocrystalline film. Equivalent circuit was optimized with the raw data, showed by dot (·), and yielded the fitting curve, showed by black line (—) (Figure 34).

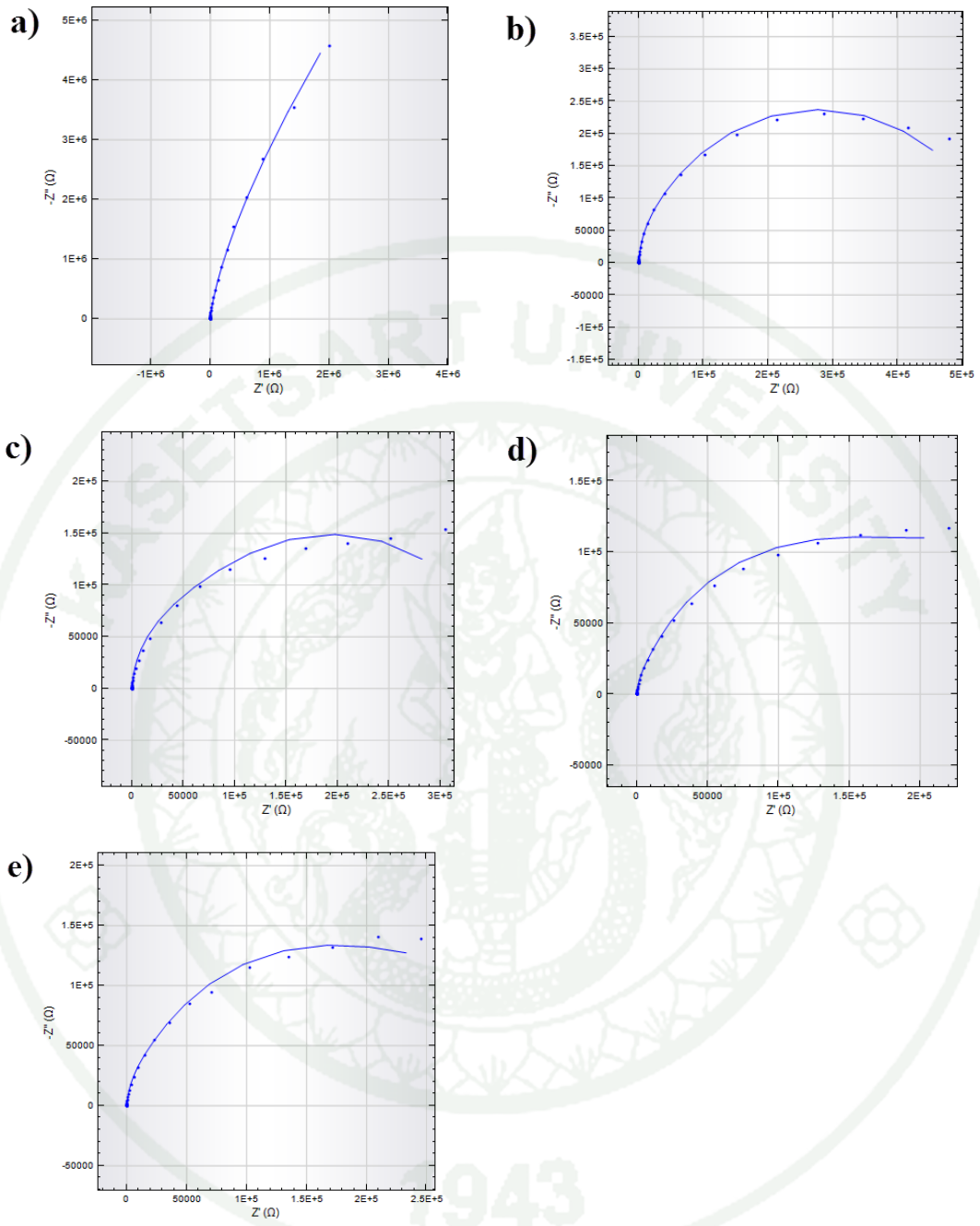

Figure 34 The fitting result shows electrical impedance signal of prepared TiO_2 electrodes, (a) P25_900, (b) P25, (c) NR-T_0.4, (d) NR-T_0.6 and (e) NR-T_0.8.

The optimized values of charge transfer resistance, R_s, R_{TiO2} and R_{FTO}, of each electrode were summarized in Table 4. The result mostly showed the agreement with the trend in the Figure 31. The calculated charge transfer resistance of the nanocrystalline TiO_2 layer of the P25 was higher than those calculated from 1-D nanostructure TiO_2 layer. The NR-T_0.6 possessed the lowest value of R_{TiO2} followed by NR-T_0.4 and NR-T_0.6. The value did not consistence with the trend of thickness of TiO_2 film.

However, the calculation showing many case of impossible results as a minus value of resistance. In general, the minus sign in the electrical circuit should be implied to the opposite direction of current flow in the circuit. Then, the absolute value can still be used to determine the value of electrical circuit elements. Accordingly, the absolute value of R_s from P25 and R_{FTO} from P25_900 are consistence with the value from other electrodes. However, the absolute value of R_{TiO2} from P25_900 is still impossible because it should be higher than R_{TiO2} of all electrodes as the higher impedance signal represented in Figure 31. The result suggested that the proposed electrical circuit would not be matched with the electrode.

Table 4 Approximated charge transfer resistance of TiO_2 thin film on FTO substrate

Electrodes	**Average film's thickness (μm)**	**Optimized resistances (Ω)**		
		R_S	R_{TiO2}	R_{FTO}
NR-T_0.4	3.2 ± 0.1	20.5	250×10^3	17.6×10^3
NR-T_0.6	5.4 ± 0.1	4.84	196×10^3	8.18×10^3
NR-T_0.8	6.8 ± 0.5	6.00	298×10^3	61.2×10^3
P25	3.2 ± 0.4	-34.5	469×10^3	41.6×10^3
P25_900	2.4 ± 0.7	22.7	-486	-2.04×10^3

CONCLUSION AND RECOMMENDATIONS

Conclusion

The fabrication of 1-D nanostructured TiO_2 on the FTO substrate electrode was successful by using the hydrothermal synthesis. The synthesized 1-D nanostructured TiO_2 obtained as the vertically aligned manner of TiO_2 nanorods with a uniformed size and shape. Parameters of the nanorod such as nanorod length (or film thickness) and the number of nanorod per unit area could be controlled by varying the concentration of Ti precursor and temperature. Crystal structure of the synthesized TiO_2 was strongly depended on the species of anion in the reaction mixture. The results indicated that the presence of Cl^- anion promoted the formation of the rutile phase TiO_2, while the anatase phase was produced from the synthesis in the presence of SO_4^{2-} ion. This method provided an advantage to produce highly pure phase of TiO_2 in a one-pot synthesis.

The vertically aligned TiO_2 nanorods on the FTO substrate only appeared from the synthesis in the presence of Cl^- ions. In the case of using other substrates such as teflon and normal glass slide, the synthesis always yielded the dandelion-like microflowers deposited on the substrate surface. The result indicated the crucial role of rutile SnO_2 layer on the FTO substrate in the formation of 1-D nanostructure.

Characterization of the rutile TiO_2 nanorod in the 1-D nanostructure TiO_2 film indicated that the rutile nanorod elongated through the [001] direction and exposed (110) plane as nanorod side wall. The small lattice mismatch between rutile TiO_2 and rutile SnO_2 and surface roughness of the polycrystalline film seemed to be the key factors which associated the nucleation of rutile TiO_2 nuclei on polycrystalline SnO_2 surface. Preferential growth of nanorod was promoted by relative surface energy of rutile, flux of growth unit and the role of Cl^-, led to the preferred orientation of TiO_2 nanorods which were confirmed by XRD analysis.

Comparison of EIS result from the 1-D nanostructured TiO_2 electrode with the nanoparticle-based electrode, P25, showed that the 1-D nanostructure TiO_2 electrode had the lower charge transfer resistance. The proposed equivalent circuit could be described the impedance signal of the prepared electrode excepted the result from P25_900. However, according to the result, the P25_900 should be the electrode that possessed the higher charge transfer resistance. Therefore, the 1-D nanostructured TiO_2 were more suitable than the mesoporous TiO_2 in term of the electron transportation.

Recommendations

In this work the using of the 1-D nanostructured TiO_2 electrode to fabricate DSSC has not been realized. The effect of 1-D nanostructured TiO_2 on DSSC efficiency will be investigated and compare with the using of mesoporous electrode. The effect of varying the film thickness and nanorod diameter on DSSC efficiency seems to be an interesting topic to study

In term of the crystallization of TiO_2 either the other kind of solvent or the using of different anion is an importance topic to study. Equally important, the using of other conductive transparent substrate such as ITO will be used to investigate the epitaxial growth.

LITERATURE CITED

Acosta, D. R., A. I. Martinez, A. A. Lopez and C. R. Magana. 2005. Titanium dioxide thin films: the effect of the preparation method in their photocatalytic properties. **J. Mol. Catal. A-Chem.** 228: 183-188.

Andrade, C., D. O. Maria, F. Tanize, H. Vitor and S. P. A. Dulcineia. 2011. Biosensors for detection of low-density lipoprotein and its modified forms, chapter 9. pp. 215-240. *In* P.A. Serra, ed. **Biosensors for Health, Environment and Biosecurity**. ISBN: 978-953-307-443-6, InTech, DOI: 10.5772/19938. Available Source: http://www.intechopen.com/books/howtoreference/biosensors-for-health-environment-and-biosecurity/biosensors-for-detection-of-low-density-lipoprotein-and-its-modified-forms, July 27, 2014.

Ansari-Rad, M., Y. Abdi and E. Arzi. 2011. Monte Carlo random walk simulation of electron transport in dye-sensitized nanocrystalline solar cells: influence of morphology and trap distribution. **J. Phys. Chem. C.** 116: 3212-3218.

Batzill, M. and U. Diebold. 2005. The surface and materials science of tin oxide. **Prog. Surf. Sci.** 79: 47-154.

Brammer, K. S., C. J. Frandsen and S. Jin. 2012. TiO_2 nanotubes for bone regeneration. **Trends. Biotechnol.** 30(6): 315-322.

Budak, S., G. X. Miao, M. Ozdemir, K. B. Chetry and A. Gupta. 2006. Growth and characterization of single crystalline tin oxide (SnO_2) nanowires. **J. Cryst. Growth**. 291: 405-411.

Cao, C., C. Hu, X. Wang, S. Wang, Y. Tian and H. Zhang. 2011. UV sensor based on TiO_2 nanorod arrays on FTO thin film. **Sensor. Actuat. B-Chem.** 156(1): 114-119.

Cao G. and D. Liu. 2008. Template-based synthesis of nanorod, nanowire, and nanotube arrays. **Adv. Colloid Interfac.** 136: 45-64.

Choi, S.K., S Kim, S. Lim and H. Park. 2010. Photocatalytic comparison of TiO_2 nanoparticles and electrospun TiO_2 nanofiber: effect of mesoporosity and interparticle charge transfer. **J. Phys. Chem. C.** 114: 16475-16480.

Comparelli, R., E. Fanizza, M. L. Curri, P. D. Cozzoli, G. Mascolo, R. Passino and A. Agostiano. 2005. Photocatalytic degradation of azo dyes by organic-capped anatase TiO_2 nanocrystals immobilized onto substrates. **Appl. Catal. B-Environ.** 55: 81-91.

Deng, Q., M. Wei, Z. Hong, X. Ding, L. Jiang and K. Wei. 2010. Selective Synthesis of rutile, anatase, and brookite nanorods by a hydrothermal route. **Curr. Nanosci.** 6: 479-482.

Diebold, U. 2003. The surface science of Titanium dioxide. **Surf. Sci. Rep.** 48: 53-229.

Dong, D., P. Li, X. Li, Q. Zhao, Y. Zhang, C. Jia and P. Li. 2010. Investigation on the photocatalytic degradation of pyrene on soil surfaces using nanometer anatase TiO_2 under UV irradiation. **J. Hazard. Mater.** 174: 859-863.

Dong, W., C. W. Lee, X. Lu, Y. Sun, W. Hua, G. Zhuang, S. Zhang, J. Chen, H. Hou and D. Zhao. 2010. Synchronous role of coupled adsorption and photocatalytic oxidation on ordered mesopourous anatase TiO_2-SiO_2 nanocomposites generating excellent degradation activity of RhB dye. **Appl. Catal. B-Environ.** 95: 197-207.

Feng, S., J. Yang, H. Zhu, M. Liu, J. Zhang, J. Wu and J. Wan. 2011. Synthesis of single crystalline anatase TiO_2 (001) tetragonal nanosheet-array on fluorine-dope tin oxide substrate. **J. Am. Ceram. Soc.** 94(2): 310-315.

Gan, X., X. Li. X. Gao, F. Zhuge and W. Yu. 2010. ZnO nanowire/TiO_2 nanoparticle photoanodes prepared by the ultrasonic irradiation assisted dip-coating method. **Thin solid films.** 518: 4809-4812.

Grattan-Bellow, P. E. 1975. Effects of preferred orientation on X-ray diffreaction patterns of gypsum. **Am. Mineral.** 60: 1127-1129.

Grätzel, M. 2005. Solar energy conversion by dye-sensitized photovoltaic cells. **Inorg. Chem.** 44: 6841-6851.

Herman, M. A. 2004. **Epitaxy: Physical Principles and Technical Implementation.** Springer, New York.

Hosono, E., S. Fujihara, K. Kakiuchi and H. Imai. 2004. Growth of submicrometer-scale rectangular parallelepiped rutile TiO_2 films in aqueous $TiCl_3$ solutions under hydrothermal conditions. **J. Am. Chem. Soc.** 126: 7790-7791.

Hsiao, P.-T., Y.-J., Liou and H. Teng. 2011. Electron transport patterns in TiO_2 nanotube arrays based dye-sensitized solar cells under frontside and backside illuminations. **J. Phys. Chem. C.** 115: 15018-15024.

Kopidakis, N., K. D. Benkstein, J. van de Lagemaat and A. J. Frank. 2003. Transport-limited recombination of photocarriers in dye-sensitized nanocrystalline TiO_2 solar cell. **J. Phys. Chem. B.** 107: 11307-11315.

Landmann, M., E. Rauls and W. G. Schmidt. 2012. The electronic structure and optical response of rutile, anatase and brookite TiO_2. **J. Phys.: Condens. Matter.** 24(19): 195503.

Li, H. and P. Afanasiev. 2011. On the selective growth of titania polymorphs in acidic aqueous medium. **Mater. Res. Bull.** 46: 2506-2514.

Li, Y., M. Guo, M. Zhang and X. Wang. 2009. Hydrothermal synthesis and characterization of TiO_2 nanorod arrays on glass substrates. **Matet. Res. Bull.** 44: 1232-1237.

Lin, J., J. Chen and X. Chen. 2011. High-efficiency dye-sensitized solar cells based on robust and both-end-open TiO_2 nanotube membranes. **Nano. Scale. Res. Lett.** 6: 475.

Linsebigler, A. L., G. Lu and J. T. Yates. 1995. Photocatalysis on TiO_2 surfaces: principles, mechanisms, and selected results. **Chem. Rev.** 95: 735-758.

Liu, B. and E. S. Aydil. 2009. Growth of oriented single-crystalline rutile TiO_2 nanorods on transparent conducting substrate for Dye-Sensitized Solar Cells. **J. Am. Chem. Soc.** 131: 3985-3990.

Liu, C. C., Y.-H. Hsieh, P.-F. Lai, C.-H. Li and C.-L. Kao. 2006. Photodegradation treatment of azo dye wastewater by UV/TiO_2 process. **Dyes Pigments.** 68: 191-195.

Lvovich, V. F. 2012. **Impedance Spectroscopy with Application to Electrochemical and Dielectric Phenomena**. John Wiley & Sons, New Jersey.

Maeda, K. and K. Domen. 2010. Photocatalytic water splitting: recent progress and future challenges. **J. Phys. Chem. Lett.** 1(18): 2655-2661.

Mali, S. S., H. Kim, C. S. Shim, P. S. Patil, J. H. Kim and C. K. Hong. 2013. Surfactant free most propable TiO_2 nanostructure via hydrothermal and its dye sensitized solar cell properties. **Sci. Rep.** 3(3004): 1-8.

Manthina, V., J. P. C. Baena, G. Liu and A. G. Agrios. 2012. ZnO-TiO_2 nanocomposite films for high light harvesting efficiency and fast electron

transport in Dye-Sensitized Solar Cell. **J. Phys. Chem. C.** 116: 23864-23870.

Martin, P. M. 2010. **Handbook of Deposition Technologies for Films and Coatings: Science, Applications and Technology.** 3rd edition. Elsevier Inc, New York.

Miao, L., S. Tanemura, S. Toh, K. Kaneko and M. Tanemura. 2004. Heating-sol-gel template process for the growth of TiO_2 nanorods with rutile and anatase structure. **Appl. Surf. Sci.** 238: 175-179.

Mu, Q., Y. Li, Q. Zhang and H. Wang. 2011. Template-free formation of vertically oriented TiO_2 nanorods with uniform distribution for organics-sensing application. **J. Hazard. Mater.** 188: 365-368.

Müller, A., M. Ghosh, R. Sonnenschein and P. Woditsch. 2006. Silicon for photovoltaic application. **Mater. Sci. Eng., B.** 134: 257-262.

Neppolian, B., H. C. Choi, S. Sakthivel, B. Arabindoo and V. Murugesan. 2002. Solar light induced and TiO_2 assisted degradation of textile dye reactive blue 4. **Chemosphere.** 46: 1173-1181.

Noack, V., H. Weller and A. Eychmüller. 2002. Electron transport in particulate ZnO electrode: a simple approach. **J. Phys. Chem. B.** 106: 8514-8523.

O'Regan, B. and M. Grätzel. 1991. A low-cost, high-efficiency solar cell based on dye-sensitized colloidal TiO_2 films. **Nature.** 353: 737-740.

Park, N.-G., J. van de Lagemaat and A. J. Frank. 2000. Comparison of dye-sensitized rutile- and anatase-based TiO_2 solar cells. **J. Phys. Chem. B.** 104: 8989-8994.

Perron, H., C. Domain, J. Roques, R. Drot, E. Simoni and H. Catalette. 2007. Optimization of accurate rutile TiO_2 (110), (100), (101) and (001) surface models from periodic DFT calculations. **Theor. Chem. Acc.** 117: 565-574.

Park, S., S.-D. Seo, S. Lee, S. W. Seo, K.-S. Park, C. W. Lee, D.-W. Kim and K. S.Hong. 2012. Sb:SnO_2@TiO_2 heteroepitaxial branched nanoarchitectures for Li ion battery electrodes. **J. Phys. Chem. C.** 116: 21717-21726.

Pottier, A., C. Chanéac, E. Tronc, L. Mazerolles and J. P. Jolivet. 2001. Synthesis of brookite TiO_2 nanoparticles by thermolysis of $TiCl_4$ in strongly acidic aqueous media. **J. Mater. Chem.** 11: 1116-1121.

Ramamurthy, V. and K. S. Schanze. 2003. **Semiconductor Photochemistry and Photophysics.** Marcel Dekker. New York.

Ranjan, S., S. Balaji, R. A. Panella and B. E. Ydstie. 2011. Silicon solar cell production. **Comput. Chem. Eng.** 35: 1439-1453.

Rosental, A., A. Tarr, A. Gerst, A. Kasikov, J. Lu, M. ottosson and T. Uustare. 2013. Epitaxial single and double nanolayers of SnO_2 and TiO_2 for resistive gas sensors. **IEEE Sens. J.** (5)13: 1648-1655.

Shang, G., J. Wu, M. Huang, J. Lin, Z. Lan, Y. Huang and L. Fan. 2012. Facile synthesis of mesoporous tin oxide spheres and their applications in dye-sensitized solar cell. **J. Phys. Chem. C.** 116(38): 20140-20145.

Shang, G., J. Wu, S. Tang, L. Liu and X. Zheng. 2013. Enhancement of photovoltaic performance of dye-sensitized solar cells by modifying tin oxide nanorods with titanium oxide layer. **J. Phys. Chem. C.** 117: 4345-4350.

Smith, B. S., S. Yoriya, T. Johnson and K. C. Popat. 2011. Dermal fibroblast and epidermal keratinocyte functionality on titania nanotube arrays. **Acta. Biomater.** 7: 2686-2696.

Song, X.-M., J.-M. Wu, M-Z. Tang, B. Qi and M. Yan. 2008. Enhanced photoelectrochemical response of a compositetitania thin film woth single-crystalline rutile nanoros embedded in anatase aggregates. **J. Phys. Chem. C.** 112: 19484-19492.

Thavasi, V., V. Renugopalakrishnan, R. Jose and S. Ramakrishna. 2009. Controlled electron injection and transport at materials interfaces in dye sensitized solar cells. **Mater. Sci. Eng. R.** 63: 81-99.

Wang, H. and J. P. Lewis. 2006. Second-generation photocatalytic materials: anion-doped TiO_2. **J. Phys.: Condens. Matter.** 18: 421-434.

Wang. H.-E., Z. Chen, Y. H. Leung, C. Luan, C. Liu and et al. 2010. Hydrothermal syntjesis of ordered single-crystalline rutile TiO_2 nanorod arrays on different substrates. **Appl. Phys. Lett.** 96: 263104 (1-3)

Wang, K., J. Zhang, L. Lou, S. Yang and Y. Chen. 2004. UV or visible light induced photodegradation of AO7 on TiO_2 particles: the influence of inorganic anions. **J. Photoch. Photobio. A.** 165: 201-207.

Wang, Y., H. Cheng, L. Zhang, Y. Hao, J. Ma, B. Xu and W. Li. 2000. The preparation, characterization, photoelectrochemical and photocatalytic properties of lantanide metal-ion-doped TiO_2 nanoparticles. **J. Mol. Catal. A-Chem.** 151: 205-216.

Wu, W. Q., B. X. Lei, H. S. Rao, Y. F. Xu, Y. F. Wang, C. Y. Su and D. B. Kuang. 2013. Hydrothermal fabrication of hierarchically anataseTiO_2 nanowire arrays on FTO glass for dye-sensitized solar cells. **Sci. Rep.** 3(1352): 1-7.

Xu, R., W. Pang and Q. Huo. 2011. **Modern Inorganic Synthetic Chemistry**. Elsevier, Amsterdam.

Yan, M., F. Chen, J. Zhang and M. Anpo. 2005. Preparation of controllable crystalline titania and study on the photocatalytic properties. **J. Phys. Chem. B.** 109: 8673-8678.

Yang, M., B. Ding, S. Lee and J.-K. Lee. 2011. Carrier transport in dye-sensitized solar cells using single crystalline TiO2 nanorods grown by a microwave-assisted hydrothermal reaction. **J. Phys. Chem. C.** 115: 14534-14541.

Yao, S. H., Y. F. Jia and S. L. Zhao. 2012. Photocatalytic oxidation and removal of arsenite by titanium dioxide supported on granular activated carbon. **Environ. Technol.** 33(9): 983-988.

Ye, M., H. Y. Liu, C. Lin and Z. Lin. 2013. Hierarchical rutile TiO_2 flower cluster-based high efficiency dye-sensitized solar cell via direct hydrothermal growth on conducting substrates. **Small.** 9(2): 312-321.

Yi, J., J. M. Lee and W. I. Park. 2011. Vertically aligned ZnO nanorods and graphene hybrid architectures for high-sensitive flexible gas sensors. **Sensor. Actuat. B-chem.** 155: 264-269.

Yoon, S.-H and J. H. Lee. 2005. Oxidation mechanism of As(III) in the UV/TiO_2 system: evidence for a direct hole oxidation mechanism. **Environ. Sci. Technol.** 39: 9695-9701.

Yu, H., J. Pan, Y. Bai, X. Zong, X. Li and L. Wang. 2013. Hydrothermal synthesis of a crystalline rutile TiO_2 nanorod based network for efficient dye-sensitized solar cell. **Chem. Eur. J.** 19: 13569-13574.

Zang, L. 2011. **Energy Efficiency and Renewable Energy Through Nanotechnology.** Springer, London.

Zhang, Q. and G. Cao. 2011. Nanostructured photoelectrodes for Dye-Sensitized Solar Cells. **Nano Today.** 6: 91-109.

Zhang, Q. and L. Gao. 2003. Preparation of oxide nanocrystals with tunable morphologies by the moderate hydrothermal method: insights from rutile TiO_2. **Langmuir.** 19: 967-971.

Zhang, Z., Md. F. Hossain and T. Takahashi. 2010. Photoelectrochemical water splitting on highly smooth and ordered TiO_2 nanotube arrays for hydrogen generation. **Int. J. Hydrogen. Energ.** 35: 8528-853.

Zhou, M., J. Xu, H. Yu and S. Liu. 2010. Low-temperature hydrothermal synthesis of highly photoactive mesoporous spherical TiO_2 nanocrystalline. **J. Phys. Chem. Solids.** 71: 507-510.

Zhong, P., W. Que, J. Zhang, Q. Jia, W. Wang, Y. Liao and X. Hu. 2011. Charge transport and recombination in dye-sensitized solar cell based on hybrid films of TiO_2 particles/TiO_2 nanotubes. **J. Alloy. Compd.** 509: 7808-7813.

Zhu, H., J. Tao, T. Wang and J. Deng. 2011. Growth of branched rutile TiO_2 nanorod arrays on F-doped tin oxide substrate. **Appl. Surf. Sci.** 257: 10494-10498.

Zhuge, F., T. Yanagida, K. Nagashima, H. Yoshida, M. Kanai, B. Xu, A. Klamchuen, G. Meng, Y. He, S. Rahong, X. Li, M. Suzuki, S. Kai, S. Takeda and T. Kawai. 2012. Fundamental strategy for creating VLS grown TiO_2 single crystalline nanowire. **J. Phys. Chem. C.** 116: 24367-24372.

APPENDICES

Appendix A

X-ray diffraction databases of rutile TiO_2, anatase TiO_2 and rutile SnO_2

Pattern: PDF 00-021-1276 Radiation: 1.54060 Quality: Star (*)

Formula	Ti O2
Name	Titanium Oxide
Name (mineral)	Rutile, syn
Name (common)	titania

Lattice:	Tetragonal	**Mol. weight =**	79.9
S.G.:	P42/mnm (136)	**Volume [CD] =**	62.43
		Dx =	
		Dm =	4.23
		I/Icor =	3.400

a =	4.59330	**alpha =**	
b =		**beta =**	
c =	2.95920	**gamma =**	
a/b =	1.00000	**Z =**	2
c/b =	0.64424		

Additional Patterns: Validated by calculated pattern
Analysis: No impurity over 0.001%
Color: White
General Comments: Pattern reviewed by Syvinski, W., McCarthy, G., North Dakota State Univ, Fargo, North Dakota, USA, ICDD Grant-in-Aid (1990). Agrees well with experimental and calculated patterns. Additional weak reflections (indicated by brackets) were observed. Naturally occurring material may be reddish brown
Optical Data Specimen location: Optical data on specimen from Dana`s System of Mineralogy, 7th Ed., I 555
Polymorphism/Phase Transition: Two other polymorphs, anatase (tetragonal) and brookite (orthorhombic), converted to rutile on heating above 700 C
Reflectance: Opaque mineral optical data on specimen from Sweden: R3R%=20.3, Disp.=Std
Sample Source or Locality: Sample obtained from National Lead Co., South Amboy, New Jersey, USA
Temperature of Data Collection: Pattern taken at 298 K
Vickers Hardness Number: VHN100=1132-1187
Unit Cell Data Source: Powder Diffraction

Primary Reference
Publication: Natl. Bur. Stand. (U. S.) Monogr. 25
Detail: volume 7, page 83 (1969)

Radiation:	CuKα1	**Filter:**	M
Wavelength:	1.54060	**d-spacing:**	
SS/FOM:	107.8 (0.0087,32)		

d	2θ	I	h	k	l
3.24700	27.447	100	1	1	0
2.48700	36.086	50	1	0	1
2.29700	39.188	8	2	0	0
2.18800	41.226	25	1	1	1
2.05400	44.052	10	2	1	0
1.68740	54.323	60	2	1	1
1.62370	56.642	20	2	2	0
1.47970	62.742	10	0	0	2
1.45280	64.040	10	3	1	0
1.42430	65.480	2	2	2	1
1.35980	69.010	20	3	0	1
1.34650	69.790	12	1	1	2
1.30410	72.410	2	3	1	1
1.27390	74.411	1	3	2	0
1.24410	76.510	4	2	0	2
1.20060	79.822	2	2	1	2
1.17020	82.335	6	3	2	1
1.14830	84.260	4	4	0	0
1.11430	87.464	2	4	1	0
1.09360	89.557	8	2	2	2
1.08270	90.708	4	3	3	0
1.04250	95.275	6	4	1	1
1.03640	96.017	6	3	1	2
1.02710	97.177	4	4	2	0
1.01670	98.514	1	3	3	1
0.97030	105.099	2	4	2	1
0.96440	106.019	2	1	0	3
0.94380	109.406	2	1	1	3
0.90720	116.227	4	4	0	2
0.90090	117.527	4	5	1	0
0.88920	120.059	8	2	1	3
0.87740	122.788	8	4	3	1
0.87380	123.660	8	3	3	2
0.84370	131.847	6	4	2	2
0.82920	136.549	8	3	0	3
0.81960	140.052	12	5	2	1
0.81200	143.116	2	4	4	0
0.78770	155.870	2	5	3	0

Pattern: PDF 03-065-5714 Radiation: 1.54060 Quality: Star (*)

Formula	Ti O2
Name	Titanium Oxide
Name (mineral)	Anatase, syn
Name (common)	

Lattice:	Tetragonal	**Mol. weight =**	79.9
S.G.:	I41/amd (141)	**Volume [CD] =**	136.3
		Dx =	3.89
		Dm =	
		I/Icor =	5.040

a =	3.78500	**alpha =**	
b =		**beta =**	
c =	9.51400	**gamma =**	
a/b =	1.00000	**Z =**	4
c/b =	2.51361		

NIST M&A collection code: A 50867 ST1243 1
Sample Preparation: Commercial pigmentary material was used
Calculated Pattern Original Remarks: Anatase-synthetic
Temperature Factor: TF Isotropic TF given by author
Unit Cell Data Source: Powder Diffraction

Structure
Publication: J. Am. Chem. Soc.
Detail: volume 77, page 4708 (1955)
Authors: Cromer, D.T., Herrington, K.
Primary Reference
Publication: Calculated from NIST using POWD-12++

Radiation:	CuKα1	**Filter:**	Not specified
Wavelength:	1.54060	**d-spacing:**	
SS/FOM:	597.3 (0.0014,35)		

d	2θ	I	h	k	l
3.51690	25.304	999	1	0	1
2.43085	36.949	56	1	0	3
2.37850	37.793	175	0	0	4
2.33256	38.566	71	1	1	2
1.89250	48.037	238	2	0	0
1.70006	53.886	148	1	0	5
1.66653	55.061	146	2	1	1
1.49330	62.107	23	2	1	3
1.48092	62.685	103	2	0	4
1.36421	68.756	49	1	1	6
1.33820	70.287	49	2	2	0
1.27917	74.053	4	1	0	7
1.26470	75.046	74	2	1	5
1.25072	76.033	20	3	0	1
1.18925	80.740	3	0	0	8
1.17230	82.156	5	3	0	3
1.16628	82.672	35	2	2	4
1.16074	83.154	15	3	1	2
1.05979	93.245	5	2	1	7
1.05152	94.203	17	3	0	5
1.04344	95.162	19	3	2	1
1.01815	98.325	11	1	0	9
1.00694	99.812	7	2	0	8
0.99659	101.237	5	3	2	3
0.95531	107.478	24	3	1	6
0.94625	108.988	12	4	0	0
0.92467	112.827	2	3	0	7
0.91917	113.868	22	3	2	5
0.91375	114.918	13	4	1	1
0.89644	118.472	35	2	1	9
0.89644	118.472	35	1	1	10
0.88894	120.117	6	2	2	8
0.88180	121.749	5	4	1	3
0.87923	122.354	15	4	0	4
0.87685	122.921	10	3	3	2
0.84635	131.050	20	4	2	0
0.84317	132.007	5	1	0	11
0.83081	135.996	3	3	2	7
0.82680	137.390	19	4	1	5
0.81257	142.878	1	4	0	6
0.81028	143.851	7	3	0	9

Pattern: PDF 01-070-6995 Radiation: 1.54060 Quality: Star (*)

Formula	Sn O2
Name	Tin Oxide
Name (mineral)	
Name (common)	tin(IV) oxide

Lattice:	Tetragonal	**Mol. weight =**	150.69
S.G.:	P42/mnm (136)	**Volume [CD] =**	71.61
		Dx =	6.99
		Dm =	
		I/Icor =	9.750

a =	4.73970	**alpha =**	
b =		**beta =**	
c =	3.18770	**gamma =**	
a/b =	1.00000	**Z =**	2
c/b =	0.67255		

ANX: AX2
Analysis: O2 Sn1
Formula from original source: Sn O2
ICSD Collection Code: 092552
Calculated Pattern Original Remarks: Stable up to 698 K (2nd ref. , Tomaszewski)
Wyckoff Sequence: f a(P42/MNM)
Unit Cell Data Source: Single Crystal

Structure
Publication: Z. Kristallogr.
Detail: volume 215, page 424 (2000)
Authors: Yamanaka, T., Kurashima, R., Mimaki, J.
Primary Reference
Publication: Calculated from ICSD using POWD-12++

Radiation:	CuKα1	**Filter:**	Not specified
Wavelength:	1.54060	**d-spacing:**	
SS/FOM:	999.9 (0.0001,31)		

d	2θ	I	h	k	l
3.35147	26.575	999	1	1	0
2.64512	33.861	804	1	0	1
2.36985	37.936	219	2	0	0
2.30977	38.962	37	1	1	1
2.11966	42.619	13	2	1	0
1.76506	51.751	587	2	1	1
1.67574	54.733	134	2	2	0
1.59385	57.802	69	0	0	2
1.49882	61.853	119	3	1	0
1.48327	62.574	1	2	2	1
1.43937	64.710	129	1	1	2
1.41557	65.935	151	3	0	1
1.35637	69.210	2	3	1	1
1.32256	71.243	62	2	0	2
1.31456	71.744	1	3	2	0
1.27389	74.412	2	2	1	2
1.21528	78.669	89	3	2	1
1.18493	81.095	27	4	0	0
1.15489	83.670	60	2	2	2
1.14955	84.148	2	4	1	0
1.11716	87.184	26	3	3	0
1.09188	89.737	71	3	1	2
1.08138	90.850	72	4	1	1
1.05983	93.240	33	4	2	0
1.03683	95.965	32	1	0	3
1.01413	98.852	1	3	2	2
1.01288	99.017	1	1	1	3
1.00570	99.980	1	4	2	1
0.95093	108.202	33	4	0	2
0.94990	108.374	63	2	1	3
0.93235	111.419	1	4	1	2
0.92953	111.930	26	5	1	0
0.91482	114.709	30	3	3	2
0.90862	115.940	65	4	3	1
0.89737	118.274	1	2	2	3
0.89237	119.358	1	5	1	1
0.88253	121.579	48	4	2	2
0.88171	121.771	36	3	0	3
0.86683	125.404	1	3	1	3
0.84840	130.447	52	5	2	1
0.83787	133.664	10	4	4	0
0.82636	137.546	37	3	2	3
0.81473	141.980	1	4	3	2
0.81285	142.758	15	5	3	0
0.81034	143.825	1	4	4	1
0.80296	147.206	47	5	1	2

Appendix B

Interpretation of the diffraction pattern

from selected-area electron diffraction (SEAD)

In this work, indexing of diffraction spots from SAED analysis was performed by using the ratio technique. This technique could be used by the condition that the crystal structure of TiO_2 nanorod was known before, as a rutile phase. The ratio technique employed the relation of camera constant

$$\frac{r}{L} = \frac{\lambda}{d}$$

Hence, at a same camera length (L) and accelerated voltage (λ), the relation between the measured distance of two diffraction spots (r) and the interplanar spacing (d-spacing) would be given by

$$\frac{r_1}{r_2} = \frac{d_2}{d_1}$$

The procedure of ratio technique was described below

1. Choosing spot1 and spot 2 which were taken a distance from the same origin spot, and then, measured the spacing, r_1 and r_2, and the angle (θ) between r_1 and r_2 (Appendix figure A1). Note that, all chosen spots should not be lying in a linear trend. In this case, the measured values were r_1 = 147.959 unit, r_2 = 159.577 unit and θ = 89.413 degree.

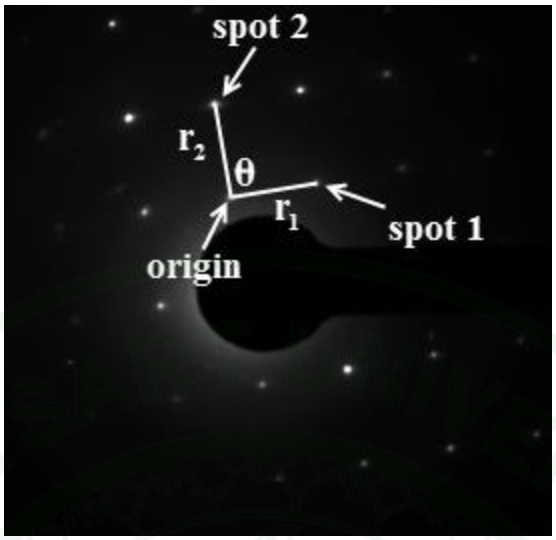

Appendix Figure B1 An illustration showing the indication of diffraction spots and measurement of r_1, r_2 and θ.

2. Taking a ratio of r_1/r_2, the calculation was obtained as $r_1/r_2 = 0.9272$

3. Prepared the table to calculated the ratio of d_2/d_1 using the d-spacing of all planes in the crystal system. D-spacing in the tetragonal rutile structure could be calculated by using the equation given below

$$\frac{1}{d^2} = \frac{h^2 + k^2}{a^2} + \frac{l^2}{c^2}$$

Appendix Table B1 Calculation of interplanar ratio (d_2/d_1) of all available crystal planes in tetragonal rutile structure.

	$(h,k,l)_2$	(110)	(101)	(200)	(111)	(210)	(211)	(220)	(002)	(310)	(221)	(301)	(112)
$(h,k,l)_1$	d-spacing (Å)	3.2470	2.4870	2.2970	2.1880	2.0540	1.6874	1.6237	1.4797	1.4528	1.4243	1.5398	1.3465
(110)	3.2470	1.0000	0.7659	0.7074	0.6739	0.6326	0.5197	0.5001	0.4557	0.4474	0.4387	0.4742	0.4147
(101)	2.4870	1.3056	1.0000	0.9236	0.8798	0.8259	0.6785	0.6529	0.5950	0.5842	0.5727	0.6191	0.5414
(200)	2.2970	1.4136	1.0827	1.0000	0.9525	0.8942	0.7346	0.7069	0.6442	0.6325	0.6201	0.6704	0.5862
(111)	2.1880	1.4840	1.1367	1.0498	1.0000	0.9388	0.7712	0.7421	0.6763	0.6640	0.6510	0.7037	0.6154
(210)	2.0540	1.5808	1.2108	1.1183	1.0652	1.0000	0.8215	0.7905	0.7204	0.7073	0.6934	0.7497	0.6556
(211)	1.6874	1.9243	1.4739	1.3613	1.2967	1.2173	1.0000	0.9622	0.8769	0.8610	0.8441	0.9125	0.7980
(220)	1.6237	1.9998	1.5317	1.4147	1.3475	1.2650	1.0392	1.0000	0.9113	0.8947	0.8772	0.9483	0.8293
(002)	1.4797	2.1944	1.6807	1.5523	1.4787	1.3881	1.1404	1.0973	1.0000	0.9818	0.9626	1.0406	0.9100
(310)	1.4528	2.2350	1.7119	1.5811	1.5061	1.4138	1.1615	1.1176	1.0185	1.0000	0.9804	1.0599	0.9268
(221)	1.4243	2.2797	1.7461	1.6127	1.5362	1.4421	1.1847	1.1400	1.0389	1.0200	1.0000	1.0811	0.9454
(301)	1.5398	2.1087	1.6151	1.4918	1.4210	1.3339	1.0959	1.0545	0.9610	0.9435	0.9250	1.0000	0.8745
(112)	1.3465	2.4114	1.8470	1.7059	1.6250	1.5254	1.2532	1.2059	1.0989	1.0789	1.0578	1.1436	1.0000

Hence, the candidate pairs were obtained by considering the value of d_2/d_1 that consistence with the ratio of r_1/r_2.

4. The candidate pairs were chosen to calculated the interplanar angle by using the equation given below

$$cos\ \theta = \frac{\frac{h_1h_2 + k_1k_2}{a^2} + \frac{l_1l_2}{c^2}}{\sqrt{\left(\frac{h_1^2 + k_1^2}{a^2} + \frac{l_1^2}{c^2}\right)\left(\frac{h_2^2 + k_2^2}{a^2} + \frac{l_2^2}{c^2}\right)}}$$

Appendix Table B2 The calculated interplanar angles of the candidate pairs

Candidated pairs	(101),(200)	(111), (210)	(220), (002)	(221), (301)	(310), (112)
Interplanar Angle (degree)	85.56	81.83	90.00	66.51	79.07

Interplanar angle between (220) and (002) planes was consistence with the measured angle, θ = 89.413. Hence, spots pattern could be indexed by the directions [110] and [001] parallel with the vector of r_1 and r_2, respectively (Figure 24b).

Appendix C

Crystal unit cell of rutile and anatase TiO_2, equilibrium morphology and the calculation of unit cell mismatch between rutile TiO_2 and rutile SnO_2

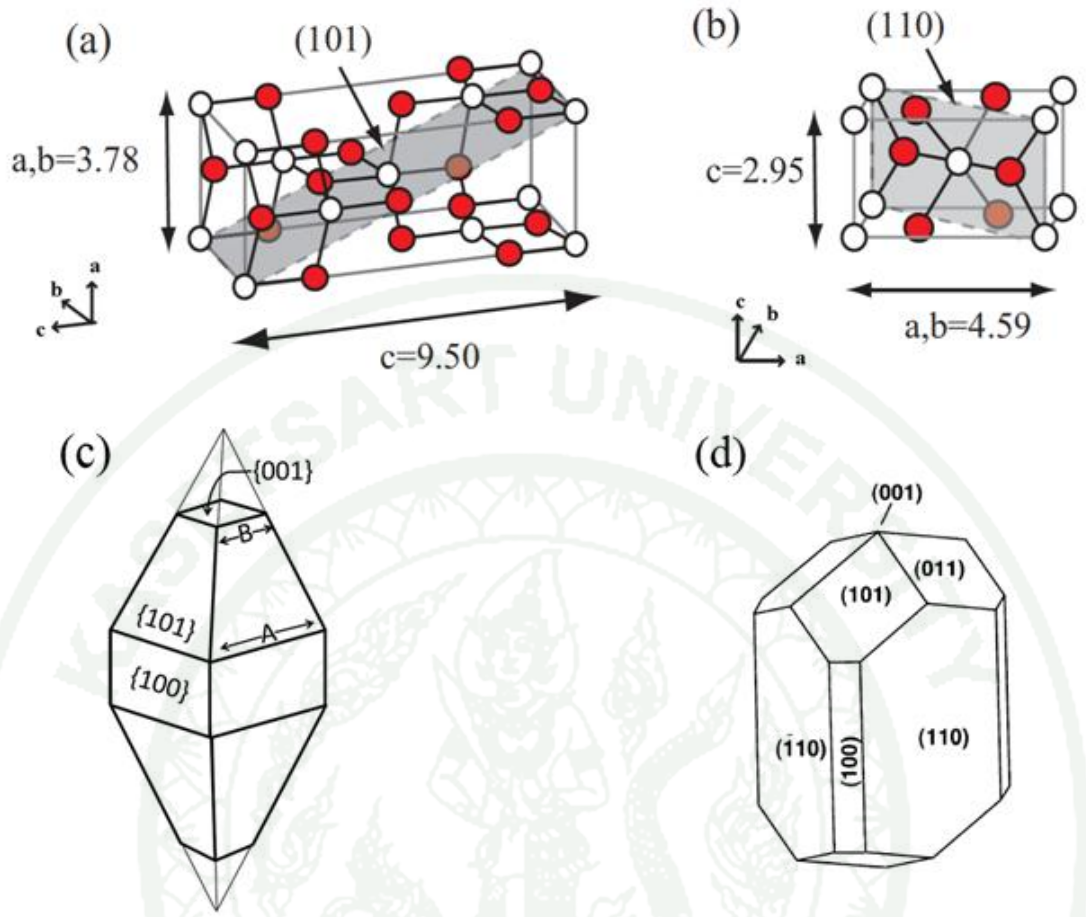

Appendix Figure C1 Crystal unit cell of tetragonal anatase TiO_2 (a) and tetragonal rutile TiO_2 (b). Oxygen and titanium atoms was shown by red and white circles, respectively. Lowest surface energy face of each were shown as the shade plane in the unit cell. Crystal morphology at equilibrium of anatase and rutile was shown in (c) and (d). Crystal structure of tetragonal rutile SnO_2 was similar to rutile TiO_2 while unit cell parameters are different (a = b = 4.7397 Å and c = 3.1877 Å).

Source: Diebold 2003; Batzil and Diebold 2005; Ishioka and Petek, 2012

Calculation of lattice mismatch between film and substrate employed the following equation (Herman, 2004)

$$Lattice\ mismatch\ = \left|\frac{\left(a_0(f) - a_0(s)\right)}{a_0(s)}\right| \times 100$$

where $a_0(f)$ and $a_0(s)$ are the lattice parameter of film and substrate, respectively.

For example, to calculate unit cell mismatch between rutile TiO_2 and rutile SnO_2, lattice parameters were equal to unit cell parameters (Diebold, 2003). Unit cell parameters of them were given as

rutile TiO_2;	a = b = 4.5933 Å	rutile SnO_2;	a = b = 4.7397 Å
	c = 2.9592 Å		c = 3.1877 Å
	(tetragonal)		(tetragonal)

lattice mismatch along a-axis (and also b-axis);

$$Lattice\ mismatch\ = \left|\frac{\left(4.5933\ \text{Å} - 4.7397\ \text{Å}\right)}{4.7397\ \text{Å}}\right| \times 100\ =\ 3.0888\%$$

lattice mismatch along c-axis;

$$Lattice\ mismatch\ = \left|\frac{\left(2.9592\ \text{Å} - 3.1877\ \text{Å}\right)}{3.1877\ \text{Å}}\right| \times 100\ =\ 7.1682\%$$

CIRRICULUM VITAE

NAME : Mr. Wanchai Deeloed

BIRTH DATE : April 5, 1989

BIRTH PLACE : Ratchaburi, Thailand

EDUCATION :

YEAR	INSTITUTE	DEGREE/DIPLOMA
2010	Kasetsart University	B.Sc. (Chemistry)

POSITION/TITLE : Postgraduate student

WORKPLACE : Faculty of Science, Kasetsart University

SCHOLARSHIP/AWARDS : The Development and Promotion of Science and Technology Talents Project (DPST)